Achromobacter xylosoxidans isolates exhibit genome diversity, variable virulence, high levels of antibiotic resistance and potential intrahost evolution.

Pooja Acharya[1], Cameron Lloyd[1], Ngoc Thien Lam[2], Jessica Kumke[1], Sreejana Ray[3], Zilia Yanira Muñoz Ramirez[4], Sanchita Das [3] and Hanh Ngoc Lam[1]

[1] Department of Biological Sciences, Virginia Tech, Blacksburg, Virginia, USA

[2] Faculty of Applied Sciences, Ton Duc Thang University, Ho Chi Minh City, Vietnam

[3] Department of Laboratory Medicine, Clinical Center, National Institutes of Health, Bethesda, MD.

[4] Facultad de Ciencias Químicas, Universidad Autónoma de Chihuahua, Campus II Circuito Universitario s/n, Chihuahua, Mexico

Running Head: A. xylosoxidans: Pathogenic Traits & Intrahost change

#Address correspondence to Hanh Ngoc Lam, hanhlam@vt.edu

1.1 Keywords

Achromobacter xylosoxidans, antibiotic resistance, virulence, secretion system, genetic diversity, intrahost evolution

2. Abstract

Achromobacter xylosoxidans is an emerging pathogen characterized by high levels of antibiotic resistance and increasing infection rates worldwide. This motile, opportunistic pathogen is widely distributed in the environment and can cause various infections, including pneumonia, bacteremia, endocarditis, meningitis, and others. In this study, we analyzed the population structure, antibiotic resistance profiles, and virulence factors of over 200 publicly available genomes. Core genome analysis revealed that *A. xylosoxidans* is highly adaptable, possessing a relatively small core genome. Antibiotic susceptibility testing of isolates from the United States revealed high resistance to multiple antibiotics. Our data show that imipenem/relebactam (IMR) is as effective against *A. xylosoxidans* as imipenem (IMI) alone, indicating that relebactam does not inhibit β-lactamase activity in *Achromobacter.* The species features multiple secretion systems, including the Type III secretion system (T3SS) of the YscN family, which is similar to those found in *Bordetella pertussis* and *Pseudomonas aeruginosa*. Isolates collected from the same patients showed changes in cytotoxicity, flagella motility, biofilm and antibiotic resistance suggesting its dynamic adaptation to host environment. Intra-host evolved isolates, NIH-010, NIH-016 and NIH-018 demonstrated the loss of flagellar motility and variable cytotoxicity while exhibiting increased antibiotic resistance and enhanced biofilm formation. Sequence analysis suggests that NIH-016-3 has tyrosine to histidine mutation at position 330 near the FlhF Guanosine triphosphate (GTP)-binding domain that may affect flagellar assembly. Interestingly, virulence assays showed significant variation in the ability of different *A. xylosoxidans* isolates to induce cell death in *in vitro* models, suggesting its dynamic adaptation to host environment.

3. Importance

This study provides a comprehensive examination of *Achromobacter xylosoxidans*, an emerging pathogen of global concern due to its high antibiotic resistance and increasing clinical relevance. By analyzing over 200 genomes, we offer critical insights into the population structure, resistance mechanisms, and virulence factors of this species. The identification of a small core genome underscores its potential for genomic plasticity. The existence of multiple secretion systems highlights the great capacity of *A. xylosoxidans* as a pathogen. Variations in virulence among *A. xylosoxidans* isolates indicate the complexity of this pathogen underscoring the need for further studies on its virulence mechanisms. Evolution within the host includes the loss of motility-associated systems and enhanced antibiotic resistance and biofilm formation. This work showed that *A. xylosoxidans* are resistant to relebactam when combined with imipenem a combination effective in other bacteria. These findings emphasize the urgent need for targeted therapeutic strategies to combat this opportunistic pathogen.

4. Introduction

The genus *Achromobacter* is a non-lactose fermenting, Gram-negative, motile bacterium recognized as an emerging pathogen in cystic fibrosis (CF) patients (1). It belongs to the β-proteobacteria class. While *Achromobacter* species are ubiquitously found in water and soil, and can grow in the plant rhizosphere, *A. xylosoxidans* isolates are primarily clinically derived (2). This bacterium was first isolated in 1971 from an ear infection (3). *A. xylosoxidans* can cause a wide range of infections, including pneumonia, bacteremia, endocarditis, meningitis, and others (4, 5). These infections, which predominantly affect immunocompromised individuals often lead to severe outcomes (4). Colonization with *A. xylosoxidans* is considered a marker of disease severity in CF patients (6) and is associated with a decline in respiratory function (7) and with a greater risk of death in lung transplant recipients (8). The persistence of *A. xylosoxidans* in both extreme environments and host organisms may be attributed to its genetic diversity and adaptability, although this aspect remains

68 poorly understood (9). Recent virulence studies have utilized various clinical isolates to explore its
69 pathogenic mechanisms (10-12). As of the time of this study, nearly 200 genomes of *A. xylosoxidans*
70 were available on NCBI. However, comprehensive analyses of the differences among isolates with
71 respect to their genomic content, virulence potential, and antibiotic resistance profiles are lacking.

72 Clinical isolates possess unique genomic features that differentiate them from environmental
73 isolates and contribute to virulence, such as the type III secretion system (T3SS), a polysaccharide
74 island, adhesion-related proteins, and several putative toxins (13). In addition to these genetic
75 elements, the Type VI Secretion System (T6SS) has been recently identified to contribute to virulence
76 alongside the T3SS (14, 15). The T3SS enables bacteria to deliver effector proteins directly into the
77 cytosol of animal or plant host cells (14). These systems have diversified into seven families,
78 spreading across Gram-negative bacteria through horizontal gene transfer (16). The T6SS facilitates
79 bacterial competition and functions as a virulence factor in various pathogenic bacteria (17, 18). In *A.*
80 *xylosoxidans*, the activity of the T6SS contributes to the internalization in immune cells wherein it
81 expresses cytotoxic effectors (11, 18). Some environmental isolates also contain phage regions
82 encoding components of type IV secretion systems (T4SS), and several genetic islands that may
83 enhance survival in host-free environments (19). In addition to secretion systems, motility is a major
84 virulence factor in pathogenic bacteria with *A. xylosoxidans* producing peritrichous flagella (20). Loss
85 of functional flagella is commonly associated with reduced virulence (21).

86 The genus *Achromobacter* is well-known for its inherent resistance to a broad range of antimicrobial
87 agents (22) and its ability to acquire resistance to commonly used treatments for respiratory
88 infections, such as fluoroquinolones, carbapenems or azithromycin (22, 23). *A. xylosoxidans* encodes
89 at least 50 drug resistance – associated genes, including β-lactamases, efflux pumps, and
90 transposons (24). Seventeen different efflux pumps have been identified in *A. xylosoxidans,* which
91 may contribute to its intrinsic resistance (24). However, to date, only four of these efflux pumps
92 have been characterized. Notably, the observed susceptibility profiles often poorly correlate with

93 the presence of putative resistance genes (24). These findings highlight the need to investigate the
94 prevalence and mechanisms of antibiotic resistance (AR) among *A. xylosoxidans* isolates (25-28).

95 In this work, we examined the genomic diversity of all available genome sequences of
96 *Achromobacter xylosoxidans*. Phylogenetic analysis was performed on a curated set of the available
97 genomes, totaling 178, including those from NCBI and our recently collected clinical isolates from
98 the NIH Clinical Center. Given the critical role of secretion systems and motility in virulence, we
99 analyzed the presence of all secretion systems (types I to IX) and flagellar system in clinical isolates.
100 Phylogenetic analysis was performed to classify the T3SS family of *A. xylosoxidans*. To examine the
101 heterogeneity of phenotypic traits in *A. xylosoxidans* across major virulence systems, we performed
102 assays to assess the ability of NIH clinical isolates to induce cytotoxicity, form biofilms, and exhibit
103 flagellar motility.

104 5. Results

105 Genomic diversity of *Achromobacter*

106 To examine the diversity among *A. xylosoxidans* isolates, we analyzed the whole-genome sequencing
107 data from 48 *Achromobacte*r spp. isolates (including 34 *A. xylosoxidans*, and other *Achromobacter*
108 species collected at the NIH clinical center in the previous study (29) referred to as NIH isolates) and
109 197 *A. xylosoxidans* genomes from NCBI (referred to as NCBI isolates). Although our focus was on *A.*
110 *xylosoxidans*, we included other *Achromobacter* species from our NIH isolates as references to
111 assess their clustering relative to *A. xylosoxidans*. The 197 NCBI isolates were predominantly from
112 the United States (n = 51), Germany (n = 39), Russia (n = 19), China (n = 12), and Australia (n = 11)
113 (Figure 1). In this dataset, *A. xylosoxidans* isolates were primarily collected from respiratory sources
114 (e.g. cystic fibrosis patients), followed by environmental samples (Figure 1A). Among the NIH
115 isolates, the majority of samples were collected from respiratory sources, with bloodstream isolates
116 being the second most common (Figure 1B).

117 From the NIH isolate sequence, genome assembly was performed and contigs greater than 500 bps
118 with coverage of 20 or more were retained. CheckM analysis identified 10 genomes with
119 contamination levels exceeding 5%, which were removed from further analysis (Table S1). We note
120 that the apparent "contamination" issue is likely due to sequencing errors. These isolates originated
121 from single colony collections and were identified as *A. xylosoxidans* based on NCBI taxonomy
122 analysis. Therefore, in later phenotypic analyses, we added back two isolates (NIH-016-1 and NIH-
123 018-3) to get a complete picture of the phenotypic changes of isolates collected from the same
124 patients. This resulted in 38 genomes from the NIH isolate dataset. For the NCBI genomes, those
125 with more than 300 contigs were excluded, and contigs shorter than 500 bps were removed, one
126 additional genome was further excluded from the NCBI dataset due to low genome completeness
127 (less than 70%) resulting in a set of 140 NCBI sequences (Table S2). This yielded a final dataset of 178
128 genomes for downstream analysis.

129 Phylogenomic analysis of all 178 isolates revealed significant diversity, with isolates largely being
130 nonclonal (Figure S1). NIH isolates were scattered among NCBI isolates, and clustering did not
131 correlate with geographical locations or sample sources. A group of environmental isolates formed a
132 distinct cluster (except for NIH-006-1), while others clustered with NIH clinical isolates, underscoring
133 the complexity of *A. xylosoxidans*. Non-*A. xylosoxidans* isolates clustered together, suggesting the
134 ability of this analysis to differentiate *Achromobacter* species. We note that two isolates classified as
135 *A. xylosoxidans* in the previous study - NIH-019-1 and NIH-021-1 (29) – were clustered with non-*A.*
136 *xylosoxidans*. A closer examination of the taxonomy analyses associated with the SRA sequences on
137 NCBI along with TYGS analysis (30), suggests that they are unlikely to be *A. xylosoxidans*. We
138 performed the average nucleotide identify (ANI) analysis and confirmed that the two isolates are not
139 *A. xylosoxidans* (Figure S2). Therefore, we excluded them from subsequent analyses involving *A.*
140 *xylosoxidans*. This resulted in a total of 22 *A. xylosoxidans* NIH isolates with the genome sequences.
141 In co-ancestry analysis, there are a few cases with some level of shared ancestry from environmental
142 samples. However, most isolates are unrelated to each other, suggesting that they are genetically

143 diverse and likely evolve independently (Figure S3). We then examined the core genome of all 162 *A.*
144 *xylosoxidans* isolates (140 NCBI and 22 NIH isolates). Using the Panaroo pipeline, we identified 2,216
145 genes present in at least 99% of the isolates, representing 34% of total genes in *A. xylosoxidans*, and
146 3,490 genes present in at least 95% of the isolates, representing 54% (Table 1). The remaining 66%
147 of genes were classified as accessory genes, highlighting the genomic plasticity of this species.

148 We also specifically looked at the phylogenetic analysis of the 22 *A. xylosoxidans* genomes from the
149 NIH isolates (Figure 1C). In this data, isolates collected from the same patient over time have the
150 same middle number. For example, NIH-016-2 and NIH-016-3 were from the same patients; or NIH-
151 010-3, NIH-010-4, NIH-010-6 were from the same patients. Initial phylogenetic analysis using two
152 methods, kSNP or Panaroo followed by RaxML (see Methods section for details) yielded identical
153 phylogenetic trees for the NIH isolates data. Using Single Nucleotide Polymorphisms (SNPs), we built
154 a phylogenetic tree of these isolates based on their SNP differences (Figure 1C). This tree showed
155 the same relationships among isolates collected from the same patients as observed with the other
156 two methods. The analysis showed that isolates collected from the same patients clustered
157 together, indicating genetic similarity and suggesting persistence and evolution within the same host
158 over time. The only exception was NIH-005-4, which did not cluster with NIH-005-2 and NIH-005-3.
159 NIH-005-4 was collected from sputum in 2014, whereas NIH-005-2 and NIH-005-3 were collected
160 from the perirectal region and bronchoalveolar lavage, respectively, in 2016.

161 **Antibiotic resistance in *Achromobacter***

162 Antibiotic susceptibility data of NIH isolates revealed a prevalence of multidrug-resistant
163 *Achromobacter* spp. among the 12 antibiotic tested, including CZA (Ceftazidime/Avibactam), C/T
164 (Ceftolozane/Tazobactam), IMR (Imipenem/Relebactam), MERO (Meropenem), AZT/ATM
165 (Aztreonam), FEP (Cefepime), TAZ (Ceftazidime), CIP (Ciprofloxacin), IMI (Imipenem), LEVO
166 (Levofloxacin), PT4/TZP (Piperacillin/Tazobactam), and SXT (Trimethoprim/Sulfamethoxazole) ((29),
167 Figure 2A). Many AR genes were identified in the NIH isolates using the Comprehensive Antibiotic

168 Resistance Database (CARD database); however, these genes could not fully explain the AR in certain
169 isolates (29). Two notable isolates, NIH-016-2 and NIH-016-3, were collected from the same patient.
170 However, NIH-016-3 was resistant to 11/12 antibiotics (all antibiotic tested except SXT), while NIH-
171 016-2 was resistant to only 3/12. Antimicrobial Resistance analysis using CZ ID website (31) showed
172 that NIH-016-2 and NIH-016-3 isolates carried similar sets of AR systems, including efflux pumps
173 (AdeFGH, AxyXY-OprZ, MexAB-OprM, MuxABC–OpmB, MexGHI-OpmD, MexCD-OprJ, MexJK-OprM,
174 MexPQ-OpmE), OXA-114h β-lactamase, AXC β-lactamase, and CatB. Thus, we re-sequenced both
175 NIH-016-2 and NIH-016-3, as well as NIH-016-1, which has the same level of antibiotic resistance as
176 NIH-016-3 and was collected after NIH-016-3. Using both short-read and long-read sequences, we
177 were able to assemble complete genomes of the three isolates. Then, variant analysis was done
178 using NIH-016-2 as a reference (Table 3). Interestingly, the variant analysis identified a T>G single
179 nucleotide polymorphism (SNP) at position 29 of *axyZ*, resulting in a nonsynonymous mutation
180 (V29G) in both NIH-016-3 and NIH-016-1. AxyZ is a negative regulator of AxyXY-OprZ RND efflux
181 pump. This mutation (V29G) is associated with overexpression of AxyXY-OprZ efflux pump, which
182 may be involved in resistance against multiple antibiotics including tobramycin, gentamicin,
183 cefepime, ofloxacin, and levofloxacin (32). SNPs that may be involved in antibiotic resistance were
184 identified in NIH-016-03 and NIH-016-01, and among these, three were of particular interest (Table
185 3). A T>A SNP at position 695 of *mutL* resulted in a non-synonymous mutation (L232Q). MutL and
186 MutS are components of the mismatch repair (MMR) system, and mutations in these genes,
187 especially MutL, are associated with a hypermutator phenotype and increased antibiotic resistance
188 in *P. aeruginosa* (33). Another variant, T>C at position 2228 in the *mfd* gene (ACP6EQ_07680) caused
189 an L743P substitution. *mfd* has been linked to elevated mutagenesis rate and the development of
190 antibiotic resistance in several bacterial species (34). Finally, a C>T SNP at position 592 of a gene
191 encoding an ABC transporter substrate-binding protein (ACP6EQ_16040) produced an R198C. ABC
192 transporters play important roles in regulating the uptake and efflux of various substrates, including

193 antibiotics (35). Overall, NIH-016-3 and NIH-016-1 appear to be hypermutator strains that allow the
194 accumulation of additional mutations, thereby enhancing the antibiotic resistance of these isolates.

195 **Secretion systems in *Achromobacter xylosoxidans* clinical isolates**

196 Previous studies have shown that *A. xylosoxidans* can express multiple virulence factors, including
197 secretion systems and flagella (14, 23). We performed a genome scan for secretion systems and
198 appendages using MacSyFinder to identify secretion systems and flagella in the 22 *A. xylosoxidans*
199 NIH isolates (Table 2). The reference genome (FDAARGOS_1091) and two additional clinical isolates
200 (GN050 and GN008) were included for comparison (Table 2). All isolates possessed T1SS, T2SS, T5SS,
201 and bacterial Tight adherence Secretion System (TadSS). T6SS was present in all isolates, and T4SS
202 was present in all isolates except NIH-009-1. Interestingly, although a number of isolates were
203 collected from the same patients over time, most of them still carry key flagella and T3SS genes.
204 Only one isolate, NIH-023-1 lost both flagellar and T3SS genes.

205 The type III secretion system is an important virulence mechanism contributing to cytotoxicity in *A.*
206 *xylosoxidans* (11, 14). Phylogenetic analysis showed that the T3SS in *A. xylosoxidans* belongs to the
207 Ysc T3SS family (Figure 3A), which includes T3SS from other pathogens such as *P. aeruginosa*,
208 *Yersinia pseudotuberculosis,* and *Bordetella pertussis*. Structural modeling of the APTase YscN from
209 *A. xylosoxidans* showed high similarity to that of *P. aeruginosa* PA14, with a root-mean-square
210 deviation (RMSD) of 0.488 A^o (Figure 3B, C). This structural similarity further supports the
211 classification of *A. xylosoxidans* T3SS within the Ysc family.

212 **Cytotoxicity in *Achromobacter***

213 To assess the cytotoxicity of the NIH isolates, we infected J774a.1 macrophages with each isolate at
214 an MOI of 7 and measured cell death over time. We included two clinical isolates, GN050 and
215 GN008, which were previously reported to exhibit differential cytotoxicity, as controls (14). The
216 result showed that the 24 isolates have variable cytotoxicity levels with NIH-018-1 being the most

217 cytotoxic, exceeding that of GN050 (Figure 4 A,B). Among clinical isolates no measurable difference
218 was detected between the isolate source. Among the isolates collected from the same patients, NIH-
219 010 and NIH-016 had minimal cytotoxicity, while all members of the NIH-025 series are cytotoxic. In
220 the NIH-018 series, the bacterial isolates appeared to have increased cytotoxicity over time, as
221 isolates collected later in the infection were more severe.

222 To further understand the basis of cytotoxicity, we examined the adherence and uptake of *A.*
223 *xylosoxidans* in macrophages. For the adherence assay, infected J774a.1 cells were washed, lysed
224 and plated for colony forming unit (CFU) counts (Figure 4C). For the uptake assay, the experiment
225 was performed similarly to the adherence assay, with an additional step of adding polymyxin B after
226 one hour of infection (Figure 4 D). Overall, the most cytotoxic isolates are the those that adhered
227 most efficiently. The NIH-018 series demonstrated the highest levels of adhesion and internalization
228 rate among our isolates, agreeing with its overall high cytotoxicity relative to all other strains. In
229 contrast, several of the least cytotoxic strains (e.g., NIH-05-2, NIH-010-4, NIH-010-3, NIH-014-1, NIH-
230 016-3, NIH-016-1, NIH-022-1 and NIH-026-1) exhibited consistently low adherence and
231 internalization in J774a.1 cells. To further assess whether cytotoxicity depend directly on bacterial
232 uptake, we performed the cell death assay in the presence of cytochalasin D on cytotoxic isolates
233 (Figure 4E). Indeed, cytochalasin D completely abolished the cell death induced by these isolates.
234 Together, these results demonstrate that internalization is a key determinant of *A. xylosoxidans*
235 cytotoxicity across clinical isolates.

236

237 **Biofilm**

238 The capacity of a bacterium to form biofilms is a strong indicator of virulence and can be tied to the
239 expression of other virulence factors (36-38). Additionally, biofilm formation improves the resistance
240 of the organism to antibiotic and environmental pressures (39). Static biofilms serve as an effective

241 method for measuring the overall capacity of a bacteria to produce biofilms and have been utilized
242 in *A. xylosoxidans* previously (40)**.** We therefore set out to examine biofilm formation in static
243 culture of *A xylosoxidans* to characterize the differences between clinical isolates. *P. aeruginosa*
244 PA01 Δ*wspF*Δ*pelA*Δ*pslBCD* was used as negative control and PA01 Δ*wspF* as a positive control (41,
245 42) for biofilm formation. GN050 showed robust biofilm formation compared to the control (Figure
246 5). Most NIH isolates demonstrated a low level of biofilm production. Only NIH-016-1, and NIH-025s
247 displayed substantial biofilm forming capabilities over the negative control. These isolates were from
248 sputum (NIH-016-1), blood or lung (NIH-025s), suggesting that the source of isolation does not
249 determine whether the bacteria can form biofilm. The intra-host series, NIH-010, NIH-016 and NIH-
250 018 do show a trend of increasing biofilm production although it's not statistically significant from
251 the *P. aeruginosa* negative control.

252 ***Achromobacter* Flagellar Motility**

253 Flagellar motility is an important virulence factor which bacteria employ to move to the site of
254 infection and is often coordinated with the expression of other virulence genes (43-45). During
255 prolonged infection, mutation in flagellar genes can accumulate resulting in an overall loss of
256 flagellar production (46). We decided to investigate the flagellar motility of our *A. xylosoxidans*
257 clinical isolates to determine if our strains demonstrate any changes in motility. Our results
258 demonstrated substantial differences in flagellar motility between strains even from isolates
259 collected from the same patients (Figure 5A). The most motile isolates are NIH-003-1, NIH-005-4,
260 NIH-014-1, NIH-016-2, NIH-018-3, and NIH-026-1. Among all 14 respiratory isolates (NIH-005-3,
261 NIH005-4, NIH009-1, NIH010-3, NIH-010-4, NIH-014-1, NIH016-2, NIH016-3, NIH018-1, NIH018-2,
262 NIH022-1, NIH023-1, and NIH025-6) 7 were identified as non-motile representing 53.8% of the
263 group. Additionally, among all non-motile isolates, 80% were isolated from a respiratory source.
264 Comparing strains isolated at different times from the same patient, NIH-005, NIH-010, NIH-016, and
265 NIH-018 series, most demonstrated a loss of motility whereas NIH-018 series showed reduced

266 motility. In NIH-005 series, isolates 2 and 3 were collected in the same year, two years after isolate 4.
267 The isolates 2 and 3 don't move while isolate 4 demonstrates high motility among all isolates. In
268 isolates NIH-010 series, isolate 6 was more motile than isolates 3 and 4, which were isolated after
269 isolate 6. In series NIH-018, NIH-018-3 is one of the best swimmers. The motility reduced about 50%
270 after one and two years in the subsequent isolates, but they are still motile. These observations
271 indicate a preference for a reduction of flagellar function in the respiratory environment.

272 The NIH-016 series demonstrated some of the most substantial differences in motility between
273 isolates (Figure 6A). In order to determine what factors may be contributing to this, we investigated
274 the genomic differences present among genomes of NIH-016 series. Multiple sequence alignment
275 between known flagellar genes in NIH-016-2 compared to the genome of NIH-016-3 showed near
276 perfect identity between the isolates except for two identified point mutations in *fliO* and *flhF*
277 (supplemental table 1). The point mutation in *fliO* when translated results in a synonymous
278 mutation. However, a T>G single nucleotide polymorphism was identified in *flhF* which resulted in a
279 Y330H mutation FlhF (Figure 6B). This mutation also exists in NIH-016-1 which was collected after
280 NIH-016-3. FlhF is a GTPase known to be important for the initial insertion of flagellar components in
281 the membrane of the bacteria. Deletion or mutations of key regions of this protein are known to
282 result in non-flagellated bacteria and thus a loss of motility (47, 48).

283 Characterization of the protein for domains by InterProScan (49) revealed a predicted SRP54-type
284 protein, GTPase domain which spans from 329 to 520. SRP54-type proteins represent signal
285 recognition particles which bind GTP and are important for trafficking to the plasma membrane (48,
286 50). This observation is in line with the predicted function of FlhF as a GTP binding protein and its
287 function in nucleating flagellar assembly in other bacteria (51, 52). Prediction of the FlhF protein
288 overall via modeling in alphafold (53) revealed four distinct structures. A structure ranging from 268
289 to 520 comprised a GTPase domain. Alphafold modeling of NIH-016-2 FlhF and NIH-016-3 FlhF and
290 subsequent alignment revealed a structural abnormality in NIH16-3's FlhF which resulted in a

291 predicted displacement of a valine at position 329 (Figure 6C). FlhF is known to homodimerize
292 following binding to GTP (50) and therefore we generated an additional model to visualize plausible
293 homodimer structures of NIH-0016-2 FlhF. Y330 was observed on the outside of the predicted
294 model, indicating that the mutation may not be causing any structural disruptions directly
295 responsible for dimerization (Figure 6D). An alternative hypothesis is the mutation may be disrupting
296 the GTP binding domain. An alignment of the predicted *Achromobacter* FlhF structure to the known
297 crystal structure of FlhF in *B. subtilis* showed a R^2 of 2.082, demonstrating they are structurally
298 similar. The known location of the GTP binding domain of *B. subtilis* FlhF is in close proximity to the
299 β-sheet containing the Y330H mutation (Figure 6E). Using observed differences in flagellar motility
300 we were able to identify a mutation in NIH-016-3 and NIH-016-1 which may be contributing to a loss
301 of flagellar motility possibly by the disruption of GTP binding.

302

303 ## 6. Discussion

304 *A. xylosoxidans* is an emerging pathogen that has garnered increasing attention in recent years.
305 Accurate identification of *Achromobacter* species has been challenging due to limited knowledge,
306 reliance on traditional and labor-intensive phenotypic identification methods, and the lack of
307 comprehensive spectra from representative species within MALDI-TOF databases (54). Advances in
308 sequencing technology and the decreasing cost of sequencing have made whole genome sequencing
309 a feasible approach for identifying *A. xylosoxidans*. Mining these whole genome sequencing data can
310 provide insights into the genetic diversity, antibiotic resistance mechanisms, and virulence potential
311 of these isolates. In this study, we analyzed publicly available sequences from NCBI and our data
312 from isolates collected at the NIH Clinical Center representing various genetic backgrounds.

313 Our core genome analysis revealed that *A. xylosoxidans* possesses a relatively small core genome
314 (34–54% of its total genes when defined as being present in 99-95% of the genomes). This is smaller

315 than the core genomes of other opportunistic pathogens such as *P. aeruginosa* and *Helicobacter*
316 *pylori*. For instance, *P. aeruginosa* has approximately 40-62% core genes - 2,503 core genes (present
317 in 100% of genomes) out of an average of 6175 genes (55), or 3,769 core genes (present in 98% of
318 genomes) out of 6103 genes (56) . Similarly, *Helicobacter pylori* has 1,227 core genes present in at
319 least 95% of the genomes (57) out of ~1,500 total genes (58), making up 81% of its genome. The
320 core genome phylogenetic tree of *A. xylosoxidans* appears to be non-clonal and isolates from the
321 same geographic locations or sample sources did not cluster together. The lack of population
322 structure and co-ancestry suggests that *A. xylosoxidans* isolates are likely evolving independently,
323 possibly under selective pressures in different environments or hosts. Such variations may arise from
324 diverse soil or water environments (where *Achromobacter* are usually found), or from differences in
325 antibiotics treatment regimens, underlying host diseases, or other health conditions. It is also worth
326 noting that we do observe an exception of a few environmental isolates that do show some level of
327 shared ancestry. Most isolates collected from the same patients clustered together and shared co-
328 ancestry (Figures 1C and S3) suggesting that they evolved from the same infection. However, an
329 exception was observed with NIH-005-4, which did not cluster with NIH-005-3 and NIH-005-2,
330 indicating that NIH-005-2 and NIH-005-3 likely represent a case of reinfection rather than a
331 persistent infection.

332 The multidrug resistance of *A. xylosoxidans* is common and concerning (Figure 2). This bacterium
333 encodes several efflux pumps, although a few have been validated. The resistance-nodulation-cell
334 division (RND)-type multidrug efflux pump, AxyABM, showed some level of resistant to
335 cephalosporins (except cefepime), aztreonam, nalidicic acid, fluoroquinolones and chloramphenicol
336 (59). Recently, a novel RND-type multidrug efflux pump, AxyXY-OprZ, was identified, which expels
337 antibiotics such as cefepime, fluoroquinolones, tetracycline or aminoglycosides including kanamycin,
338 gentamicin, and tobramycin (60). Additionally, a recent study discovered the presence of another
339 narrow-spectrum RND-type multidrug efflux pump, AxyEF-OprN, which pumps out fluoroquinolones,
340 tetracyclines, and carbapenems (40). An additional study identified AxySUV in some of the *A.*

341 *xylosoxidans* genomes that export fluoroquinolones (ciprofloxacin, levofloxacin), carbapenems
342 (doripenem), tetracycline (doxycycline, minocycline), and chloramphenicol (61). In addition to the
343 presence of various efflux pumps, intrahost evolution may contribute to increasing antibiotic
344 resistance over time. One interesting case is the NIH-016 series. NIH-016-3, collected seven months
345 after NIH-016-2 from the same patient, exhibits higher AR and enhanced biofilm formation
346 compared to NIH-016-2. Phylogenetic analysis confirms their close relationship, suggesting that NIH-
347 016-3 evolved from NIH-016-2. While both isolates carry similar sets of resistance genes identified
348 from the CARD database and CZ ID website, NIH-016-3 demonstrates greater resistance to
349 antibiotics. Comparing single nucleotide polymorphism of all three isolates in the series suggest that
350 the later collected isolates accumulated mutations DNA mismatch repair systems and in several
351 efflux pump. Hypermutators may exhibit greater resistance because their elevated mutation rate
352 leads to additional mutations in genes that contribute to antibiotic resistance. It is possible that the
353 hypermutator emerged first, followed by mutations in efflux pumps and transporters, ultimately
354 resulting in broad resistance to multiple antibiotics.

355 In our NIH isolates, 21% of isolates are resistant to IMI while 34% isolates are resistant to IMR.
356 Relebactam, a wide-spectrum β – lactamase inhibitor against class A (extended-spectrum
357 β–lactamases KPC) and class C (AmpC) β–lactamases, does not seem to work in *Achromobacter*. In
358 fact, all NIH isolates that were resistant to IMI were also resistant to IMR. In other bacteria such as
359 *Pseudomonas* and *Klebsiella*, IMR was more effective than IMI (62, 63). This could be because *A.*
360 *xylosoxidans* possesses other β–lactamases classes. NIH-016s possess AXC family carbapenem-
361 hydrolyzing class A β–lactamase and OXA-114 family class D β–lactamase. The OXA-114 may help
362 *Achromobacter* to escape relebactam when used in combination with imipenem. These findings
363 highlight that *A. xylosoxidans* employ multiple AR genes and strategies, which require further
364 research.

365 As secretion systems are key virulent factors in bacteria, we investigated the presence of all possible
366 secretion systems in the NIH isolates. T1SS, T2SS, T5SS, and bacterial Tight adherence Secretion
367 System (TadSS) were identified in all isolates. T1SS is capable of transporting unfolded substrates,
368 including digestive enzymes (proteases and lipases), adhesins, heme-binding proteins, and proteins
369 with repeats-in-toxins (RTX) motifs (64). T2SS, a secretion machinery prevalent in many Gram-
370 negative bacteria, facilitates the secretion of virulence factors such as proteases, toxins, lipases, and
371 carbohydrate-degrading enzymes, which aid the survival of both pathogenic and environmental
372 bacteria (65). T5SS is involved in the secretion of virulence proteins critical to pathogenesis in several
373 bacteria, including immunoglobulin A protease of *Neisseria gonorrhoeae (66)*, IcsA protein of
374 *Shigella flexneri* (67), and YadA of *Yersinia enterocolitica (68)*. TadSS is an important secretion system
375 that supports infection, cell adherence, competence, and biofilm formation in many pathogenic
376 bacteria, such as *P. aeruginosa*, *Bordetella pertussis*, *Burkholderia pseudomallei*, and *Mycobacterium*
377 *tuberculosis* (69). The presence of these secretion systems in all isolates suggests that they all have
378 the potential to be pathogenic.

379 Most isolates have T3SS, T4SS, T6SS and flagella. T3SS is associated with the cytotoxicity of the
380 isolates (14). AxoU is the only known T3SS substrate that is responsible for host cell cytotoxicity in *A.*
381 *xylosoxidans*. All cytotoxic isolates carried both T3SS and AxoU. T4SS is primarily involved in
382 horizontal genetic transfer (HGT) between different microorganisms, which may contribute to
383 pathogenesis and antibiotic resistance (15). T6SS is a multiprotein complex that uses a spring-like
384 mechanism to deliver effector proteins into target cells (70). In *A. xylosoxidans,* T6SS plays a role in
385 targeting competing bacteria and is crucial for the internalization of the pathogen into lung epithelial
386 cells (15). Flagella, which are evolutionarily related to T3SS, play roles in motility, surface adherence
387 and biofilm formation (71). Interestingly, while most isolates encode flagellar genes, only 59% of
388 them are motile, suggesting an adaptation strategy of the isolates that are isolated over a long
389 period of time from a patient indicating chronic carriage/infection. A study on the genotypic and
390 phenotypic evolution of the *A.xylosoxidans* isolates collected from CF patients over time showed a

391 decrease in swimming motility, an increase in antibiotic resistance, and enhanced biofilm formation
392 in evolved strains (72).

393 Phylogenetic analysis indicates that the T3SS of *A. xylosoxidans* structurally belongs to the Ysc family
394 of T3SS systems, which includes *Bordetella* spp. (alpha-proteobacteria), *Yersinia* spp., *P. aeruginosa*,
395 *Aeromonas* spp., *Photorhabdus luminescens*, and *Vibrio* spp. (gamma-proteobacteria) (Figure 4). In
396 *Bordetella spp*., *Yersinia* spp., and *Photorhabdus luminescens,* the T3SS confers resistance to the
397 innate immune response by inhibiting phagocytosis, leading to extracellular localization of the
398 pathogens (73-75). While *P. aeruginosa* is known as an extracellular pathogen, it can replicate
399 intracellularly where T3SS and its effectors (mainly ExoS) play critical roles in internalization, vacuole
400 escape, evasion of inflammasome and autophagy as well as bleb formation prior to detachment (76).
401 Similarly, T3SS is important for *Aeromonas* and *Vibrio* to maintain its intracellular niches (77, 78). In
402 *A. xylosoxidans,* survival within macrophages for several hours is independent of T3SS; however,
403 cytotoxicity depends on the presence of T3SS (11, 12). AxoU is the only known T3SS substrate linked
404 to host cell lysis (14), although other T3SS effectors may be secreted during infection, as disrupting
405 the T3SS (e.g., *sctV*) prevents cell death, whereas disruption of *axoU* alone does not (11).
406 Interestingly, T3SS and *axoU* are expressed shortly after infection (within 30 minutes), but are
407 subsequently turned off (11). Whether T3SS is reactivated when the bacteria escape the vacuole and
408 lyse the host cells remain to be tested. Additional characterization of the T3SS and other virulence
409 systems are required to identify other effectors and their role in infection and survival.

410 Our clinical isolates demonstrate substantial heterogeneity in their cytotoxicity (Figure 4). *A.*
411 *xylosoxidans* cytotoxicity is conducted through its T3SS with the major effector known to cause cell
412 death being AxoU, a homologue of ExoU found in *P. aeruginosa* (79). While most isolates carry T3SS
413 and AxoU, more than 50% of isolates were non-cytotoxic, suggesting a complex regulation of T3SS
414 expression. Multiple sequence alignment of promoter regions of T3SS genes suggests a loss of the
415 *sctB* promoter in both GN008 and NIH-016-2. *sctB* encodes a T3SS translocon protein required for

416 effector injection into host cells (80); therefore, its absence is expected to reduce T3SS - dependent
417 cytotoxicity. Recent work showed that transcription of *axoU* was upregulated in GN050, but not in
418 GN008, shortly after phagocytosis (14). Together these observations suggest that transcriptional
419 regulation may be one mechanism controlling T3SS expression in these isolates.

420 The ability of *A. xylosoxidans* to adhere to host cells and undergo phagocytosis is known to be
421 integral to its cytotoxic activity (11, 14). Multiple virulence factors have been implicated in
422 contributing to this phenotype, including the T6SS and the adhesin ArtA (12, 15). Consistent with
423 previous findings, our data showed that cytotoxicity across isolates required bacterial uptake (Figure
424 4). There was no observable relationship between overall flagellar motility and cytotoxicity but an
425 association with biofilm production and cytotoxicity (Figure S4). In NIH-018 series, there was an
426 increase in cytotoxicity from isolates collected after the others (Table 2). This is interesting, as in
427 other bacteria, the bacteria tend to get less virulent when they colonized the host for a long time
428 (81, 82). It is possible that *in vitro* cytotoxicity is not fully correlated with *in vivo* virulence, which
429 remains to be tested.

430 Biofilm production is another major aspect of the bacterial lifestyle. Production of biofilm is
431 important in promoting bacterial resistance to environmental pressures and defending against
432 immune cells during infection (39, 83). Biofilm formation can contribute significantly to antibiotic
433 resistance, as the biofilm matrix provides a protective environment that limits antibiotic penetration
434 and promotes the survival of persistent cells (84). While many methods for observing biofilm
435 formation exist, we chose to adopt static biofilm formation as it allowed for the high throughput
436 monitoring of our available strains. Additional methods such as flow cell and micro biofilm formation
437 are available and provide additional context for development and maintenance of biofilms, however
438 as a diagnostic tool static biofilms are commonly used to monitor the overall production of biofilms
439 in bacteria, and indeed in *A. xylosoxidans* (85). The NIH isolates produce low level of biofilm in
440 general (Figure 6). We observed a slight increase in biofilm production in the intrahost isolates, NIH-

441 010s, NIH-016s and NIH-018s although the difference was not significant. GN050 collected from ear
442 effusion (14), is the only isolate that produced robust biofilm. It could be that because most of our
443 isolates were from respiratory tract, they don't form as much biofilm. Alternatively, biofilm was
444 tightly regulated, and we didn't assay the bacteria in the desired condition for biofilm formation in
445 these particular isolates. Biofilm production was not correlated with motility or antibiotic resistance
446 (Figure S4), although the strong biofilm former are moderately motile.

447 Flagellar motility in bacteria is commonly associated with increased disease severity and
448 pathogenesis. Multiple related species such as *Bordetella* and *Pseudomonas* are known to have the
449 expression of virulence systems such as the T3SS modulated by the expression of the flagella (45, 86)
450 . Additionally, bacteria with dysfunctional flagella are known to have reduced pathogenicity *in vivo*
451 due to the inability to reach the site of infection (44). Bacteria isolated from the lungs are known to
452 preferentially gain mutations in the flagella resulting in non-motile genotypes as compared to other
453 sites of infection (37, 46). We identified a mutation in *flhF* which we hypothesize could result in a
454 loss of flagellar production. We observed no correlation between overall motility and cytotoxicity
455 (Figure S4). Interestingly, isolates that are the most cytotoxic are motile, but the most motile isolates
456 are not cytotoxic. It could be possible that the most motile isolates can escape phagocytosis in our *in*
457 *vitro* infection model. Strains that experience a loss of either flagellar motility or cytotoxicity do not
458 experience a relative loss in the other. It is unclear what role the flagella of *A. xylosoxidans* plays
459 during infection. In multiple bacterial species the function of the flagella is highly correlated with the
460 activity of virulence mechanisms. The regulatory relationship between motility and virulence varies
461 substantially between organisms. *Bordetella spp.* display an inverse relationship (86), whereas
462 *Pseudomonas aeruginosa* displays a positive relationship between T3SS production and flagellar
463 motility (45). *Salmonella spp.* also demonstrate a positive relationship with the SPI-1 T3SS but not
464 the SPI-2 T3SS (87). These observations indicate a general positive correlation between flagella and
465 virulence factor expression in extracellular pathogens. In *A. xylosoxidans,* T3SS expression seemed to
466 increase shortly after the bacteria are phagocytosed by macrophage but dampened quickly.

467 Whether T3SS is shut off and then gets re-activated at later stage of infection or it remains
468 functional to some extend without making more apparatus and elevated level of substrate
469 production requires further investigations.

470 In summary, this study highlights the genetic and phenotypic diversity among *A. xylosoxidans*
471 isolates, as evidenced by the high accessory genome content and variability in secretion systems.
472 Significant differences in antibiotic resistance and virulence mechanisms underscore the adaptability
473 of this bacterial species. These findings emphasize the need for further mechanistic studies to
474 elucidate the pathogenicity and antibiotic resistance mechanisms of *A. xylosoxidans*.

475

476 ## 7. Methods

477 **Data used in this work:**

478 Raw sequence data from Bio Project ID PRJNA1148967, referred to as NIH data with 38
479 *Achromobacter xylosoxidans*, *A. denitrificans, A. ruhlandii, A. mucicolens and A. insolitus* genomes.
480 197 genomes of *Achromobacter xylosoxidans* from NCBI
481 (https://www.ncbi.nlm.nih.gov/datasets/genome/?taxon=85698&assembly_level=1:3) as of
482 September 2024, referred as NCBI data.

483 **Sources of Bacterial Strains**

484 All NIH strains used in phenotypic studies were obtained from the NIH Clinical Center and were
485 published in a recent work (29). GN050 and GN008 were provided by Dara Frank and have been
486 previously published (14). PA01 Δ*wspF*Δ*pelA*Δ*pslBCD* and PA01 Δ*wspF* were previously published
487 (88).

488 **Genome assembly**

489 For all NIH isolates: Adapters were trimmed using Trimmomatic version V0.39 (89) with default
490 parameters, except the last 10 bases were removed. FastQC (v0.11.9) (90) was used to visualize read
491 quality, which showed an average base sequence quality greater than 28 across the reads. Genome
492 assembly was performed using SPAdes (91) in careful mode. The quality of the assemblies was
493 evaluated using QUAST (v5.2.0) (92), which provided metrics such as number of contigs, length, and
494 N50.

495 **Genome filtering**

496 For NIH data, contigs shorter than 500 base pairs or with coverage below 20x were removed. For
497 NCBI data, genomes with more than 300 contigs were excluded, and contigs shorter than 500 base
498 pairs were removed. Potential sample contamination was assessed using CheckM (v1.2.3) (93).
499 Genomes with contamination levels exceeding 5% or completeness below 90% were excluded from
500 subsequent analyses.

501 **Average Nucleotide Identity (ANI)**

502 The complete genome sequences of *A. xylosoxidans* strains GCA_013282235.1 (GN050) and
503 GCA_013282255.1 (GN008) were included for comparison. ANI analysis was performed using the
504 ANIm method described previously (94) and implemented in the Python
505 module pyANI (tps://github.com/widdowquinn/pyani). ANI values were calculated for all 24 NIH
506 genomes and the two reference strains using pyANI version 0.3.0-alpha with MUMmer-based
507 alignments and graphical output enabled. ANI percentage identity was used to define the different
508 clusters.

509

510 **Core genome analysis**

511 Assembled genomes were annotated with Prokka (1.14.6) (95) with the annotation from assembly
512 ASM1672882v1 (strain FDAARGOS_1091) used as a reference database. Core genome analysis was
513 performed using the Panaroo pipeline version 1.5.0 (96) with a protein sequence identity threshold
514 of 90%, gene length coverage cutoff of 75%, and a core genome sample threshold of 0.95.

515 **Initial phylogenetic analysis of *Achromobacter xylosoxidans***

516 Phylogenetic analysis of NIH and NCBI data was performed using kSNP4 (97). The optimal k-mer size
517 was determined using Kchooser. kSNP4 was run with the selected k-mer size, and a parsimony tree
518 was generated based on SNP loci present in at least 95% of the genomes. For NIH data, in addition to
519 kSNP4, RaxML (98) was used to construct the phylogenetic tree. Briefly, core genes identified by
520 Panaroo were used as input. RAxML v8.2.12 (98) was utilized to build a rooted maximum likelihood
521 tree using the general time-reversible (GTR) substitution model with gamma correction to account
522 for rate variation among sites. Since the phylogenetic trees generated by kSNP4 and RAxML were
523 identical, only one tree was reported. The final tree was visualized using iTOL (99).

524 **Phylogenetic analysis with SNPs**

525 To determine the phylogenetic relationships among the *A.xylosoxidans* isolates, the core genome
526 alignment generated by Panaroo was used to identify core genome SNPs with SNP-sites (100). SNP
527 alignment was then used to construct a maximum likelihood phylogenetic tree with IQ-TREE version
528 2.4 (101), employing ModelFinder Plus for model selection, ultrafast bootstrap analysis with 1000
529 replicates, and the approximate likelihood ratio test with 1000 replicates. The final tree was
530 visualized and annotated using iTOL (https://itol.embl.de/).

531

532 **Population structure analysis**

533 The genome-wide haplotype data were calculated as described previously (102). SNP calling was
534 performed for core genes identified by the panaroo pipeline, and imputation for polymorphic sites
535 with a missing frequency of less than <1% was conducted using BEAGLE v.3.3.2 (103). This genome-
536 wide haplotype dataset contained 144,290 SNPs, which was used to define isolate populations and
537 subpopulations based on haplotype profile similarity. fineSTRUCTURE analysis (104) was performed
538 with 200,000 iterations of both the burn-in and Markov chain Monte Carlo (MCMC) method to
539 cluster individuals based on the coancestry matrix, as previously described (105). The results were
540 visualized as a heat map, with each cell representing the proportion of DNA a recipient receives from
541 each donor.

542 **Variant calling**

543 The variants were called with Snippy v4.4.0 (https://github.com/tseemann/snippy), with default
544 option. NIH-016-2, collected first in the NIH-016 series, was used as a reference.

545 **Secretion system analysis**

546 Secretion systems and appendages were identified using MacSyFinder 2.1.3 (106). TXSScan was run
547 to search for all types of secretion systems and appendages, including T1SS, T2SS, T3SS, T4SS, T5SS,
548 T6SS, Flagellum, Tad pilus, and T9SS. CONJScan was run to detect conjugative and mobilizable
549 elements, which include T4SSs. The "ordered replicon" option was used for our complete genome
550 sequences.

551 For genomes in which the secretion systems were not found by MacSyFinder, we manually looked
552 up for key genes of the systems in the annotated genomes, as it is possible that the segmentation of
553 the sequences that feed into MacSyFinder interferes with the gene search. These are also key genes
554 used by MacSyFinder. A system was noted as absent when none of the genes were found.

555 **Phylogenetic analysis of T3SS**

556 Amino acid sequences of SctN or its homologs were extracted from Uniprot and NCBI. Multiple
557 sequence alignment of SctN sequences was performed using MAFFT (107) with default parameters.
558 A rooted maximum likelihood tree was constructed using RAxML v8.2.12 (98) with the general time-
559 reversible (GTR) substitution model and gamma correction for rate variation among sites. The
560 phylogenetic tree was visualized using iTOL (99).

561 **Structural Modeling of YscN ATPase**

562 The amino acid sequence of the T3SS ATPase from *A. xylosoxidans* was obtained from NCBI with
563 sequence ID of WP_020925211.1. Structure of YscN was predicted using AlphaFold via the website:
564 https://alphafoldserver.com/. The predicted structure of *Pseudomonas aeruginosa* PA14 was
565 downloaded from https://alphafold.ebi.ac.uk/entry/A0A2U2Y0I4 with accession number of AF-
566 A0A0H2Z9F1-F1. Structural alignment of the two proteins was performed using Pymol (The PyMOL
567 Molecular Graphics System, Version 3.0 Schrödinger, LLC).

568 **Antibiotic susceptibility testing**

569 Broth microdilution testing was carried out using two commercial Sensititre™ panels: the Gram-
570 Negative Non-Fermenters MIC Plate and the Gram Negative MDRGN2F AST Plate (Thermo Fisher
571 Scientific). Each isolate was adjusted to a 0.5 McFarland standard in Sensititre demineralized water
572 and then transferred into Sensititre™ Mueller–Hinton Broth with TES. The panels were inoculated
573 using the Sensititre™ AIM™ automated inoculation system and incubated in the Sensititre™ ARIS
574 HiQ™ instrument according to the manufacturer's instructions. After incubation, plates were
575 automatically read by the system and then manually confirmed using the Sensititre™ Vizion™ Digital
576 MIC Viewer. Quality control strains included *E. coli* ATCC 25922 and ATCC 35218, *P. aeruginosa* ATCC
577 27853, and *K. pneumoniae* ATCC 700603. MIC values were interpreted using CLSI breakpoints for
578 Other Non-Enterobacterales (CLSI M100, 33rd edition, 2023).

579

580 **Biofilm**

581 Bacterial cultures were initiated in glass culture tubes by inoculating bacteria from LB agar plates
582 into 1 mL of LB broth at a starting OD600 of 0.1. The cultures were then incubated statically at 37°C
583 for 3 days. On the third day, media was removed by pipetting, and biofilms were washed with water
584 and dried overnight at 37°C. The following day, a 1% crystal violet solution was used to stain biofilms
585 for 5 minutes, followed by additional washes with water and overnight drying at 37°C. Biofilms were
586 solubilized with 100% DMSO, and absorbance was measured at 595 nm using a BioTek plate reader.

587 **Infection of *Achromobacter* in cell lines**

588 J774a.1 cells were seeded at a density of $6x10^4$ cells in 100 µL DMEM media in a tissue culture-
589 treated black flat-clear bottomed 96-well plate. On the day of infection, cells were washed with PBS
590 and incubated for one hour with OPTI-MEM media containing 200 ng/mL propidium iodide (PI) and
591 1.45µM Hoechst 33342. *Achromobacter* inoculum was then prepared by resuspending bacteria in
592 OPTI-MEM. Cells were infected with the bacteria at multiplicity of infection of 7 and spun down at
593 750 rpm for 5 minutes to synchronize infection. The 96-well plate was then inserted into a stage
594 incubator supplied with CO_2 and maintained at 37°C in a Nikon AXR confocal fluorescent microscope.
595 Three images of cells were taken at arbitrary locations within each well and observed every hour for
596 up to five hours. Cytotoxicity was measured by the ratio of PI^+ signal to $Hoechst^+$ signal (dead
597 cells/total cells) expressed in percentage using ImageJ v 1.54g. PI^+ and $Hoechst^+$ cells were processed
598 using background subtraction, followed by gamma adjustment and median filtering. Then, Otsu
599 method was applied for thresholding (108), and cell counts were obtained using the Analyze
600 Particles function.

601 **Adhesion and Internalization assays**

602 J774a.1 cells were put down onto a cell culture treated 96 well plate at $6x10^4$cells/well in 100µL
603 DMEM to grow overnight. At the day of infection, the media from the wells was replaced with media

604 containing 1µL DMSO/mL DMEM or 2µg/mL cytochalasin D as a negative control. After 1 hour of
605 incubation bacterial strains grown at 37^0C then room temperature for one day each were inoculated
606 onto the cells at an MOI of 7. After 1 hour of incubation at 37^0C the media was removed, and the
607 cells were washed twice with 100µL PBS. Cells which were treated with 1µL DMSO/mL DMEM had
608 media replaced with either 1µL DMSO/mL DMEM (adherence) or with 1µL DMSO+50µg Polymyxin
609 B/mL DMEM (internalized bacteria). Cells treated with 2µg/mL cytochalasin D had media replaced
610 with 2µg cytochalasin D + 50µg Polymyxin B /mL (negative control). After one hour of incubation at
611 37^0C the media was removed and 100µL 0.1% SDS was added and incubated at room temperature
612 for 15 minutes. The resulting bacterial suspension was serially diluted and CFUs were measured by
613 spot plating 5µL of dilutions onto LBA.

614 **Swimming motility in *Achromobacter* strains**

615 Bacteria were inoculated and grown overnight in 1mL LB broth from single colonies on LB agar
616 plates. Overnight growth was measured by OD600 and concentrated to an OD600 of 10 in 100µL.
617 2µL of the resulting suspension was injected via pipette into 0.25% agarose 2% tryptone plates.
618 Plates were incubated at 37^oC for 4 hours and imaged with a Chemidoc^{tm} Imaging System using the
619 stain free blot procedure with 3 second exposure time. The resulting images were exported to
620 ImageJ. Images were converted to an 8-bit format, and a brightness/contrast correction step was
621 performed. The zone of motility was then selected using the circle tool and resulting area in Pixels
622 was exported. Pixel count was converted to mm^2 using the formula: mm^2 = (Pixels)/(5000 Pixels
623 /((3.5mm/2)^2*3.14159)).

624 **Statistical analysis**

625 All statistical analyses were performed in GraphPad Prism version 10. Data were assessed for
626 normality using the Shapiro-Wilk test. For comparisons among multiple groups, one-way ANOVA
627 with Dunnett's post hoc test was used for normally distributed data, while the nonparametric

Kruskal-Wallis test followed by Dunn's multiple comparisons test was used for nonparametric data. Data are presented as mean ± SD unless otherwise stated.

8. Author statements

8.1 Author contributions

Pooja Acharya (Formal Analysis, Data Curation, Methodology, Writing), Cameron Lloyd (Formal Analysis, Methodology, Writing), Ngoc Thien Lam (Formal Analysis, Writing), Jessica Kumke (Formal Analysis), Sreejana Ray (Resources), Zilia Yanira Muñoz Ramirez (Formal Analysis), Sanchita Das (conceptualization, resources) and Hanh Ngoc Lam (Conceptualization, Data Curation, Formal Analysis, Funding Acquisition, Investigation, Methodology, Supervision, Writing)

8.2 Conflicts of interest

The author(s) declare that there are no conflicts of interest

8.3 Funding information

This work is supported by NIH R00AI139281.

This research was supported [in part] by the Intramural Research Program of the National Institutes of Health (NIH). The contributions of the NIH author(s) were made as part of their official duties as NIH federal employees, are in compliance with agency policy requirements, and are considered Works of the United States Government. However, the findings and conclusions presented in this paper are those of the author(s) and do not necessarily reflect the views of the NIH or the U.S. Department of Health and Human Services.

8.4 Acknowledgements

We thank Dara Frank (medical College of Wisconsin) for sharing the GN050 and GN008 strains.

650 ## 9. References

651 1. Veschetti L, Boaretti M, Saitta GM, Passarelli Mantovani R, Lleo MM, Sandri A, et al.
652 Achromobacter spp. prevalence and adaptation in cystic fibrosis lung infection. Microbiol Res.
653 2022;263:127140.
654 2. Jeukens J, Freschi L, Vincent AT, Emond-Rheault JG, Kukavica-Ibrulj I, Charette SJ, et al. A
655 Pan-Genomic Approach to Understand the Basis of Host Adaptation in Achromobacter. Genome Biol
656 Evol. 2017;9(4):1030-46.
657 3. Yabuuchi E, Oyama A. Achromobacter xylosoxidans n. sp. from human ear discharge. Jpn J
658 Microbiol. 1971;15(5):477-81.
659 4. Swenson CE, Sadikot RT. Achromobacter respiratory infections. Ann Am Thorac Soc.
660 2015;12:252-8.
661 5. Jakobsen TH, Hansen MA, Jensen PØ, Hansen L, Riber L, Cockburn A, et al. Complete
662 Genome Sequence of the Cystic Fibrosis Pathogen Achromobacter xylosoxidans NH44784-1996
663 Complies with Important Pathogenic Phenotypes. PLoS ONE. 2013;8(7):e68484.
664 6. Esposito S, Pisi G, Fainardi V, Principi N. What is the role of Achromobacter species in
665 patients with cystic fibrosis? Front Biosci (Landmark Ed). 2021;26(12):1613-20.
666 7. Tetart M, Wallet F, Kyheng M, Leroy S, Perez T, Le Rouzic O, et al. Impact of Achromobacter
667 xylosoxidans isolation on the respiratory function of adult patients with cystic fibrosis. ERJ Open Res.
668 2019;5(4).
669 8. Somayaji R, Stanojevic S, Tullis DE, Stephenson AL, Ratjen F, Waters V. Clinical Outcomes
670 Associated with Achromobacter Species Infection in Patients with Cystic Fibrosis. Ann Am Thorac
671 Soc. 2017;14(9):1412-8.
672 9. Nielsen SM, Penstoft LN, Nørskov-Lauritsen N. Motility, Biofilm Formation and Antimicrobial
673 Efflux of Sessile and Planktonic Cells of Achromobacter xylosoxidans. Pathogens. 2019;8(1):14.
674 10. Wills BM, Garai P, Riegert MO, Sanchez FT, Pickrum AM, Frank DW, et al. Identification of
675 Virulence Factors Involved in a Murine Model of Severe Achromobacter xylosoxidans Infection.
676 Infect Immun. 2023;91(7):e0003723.
677 11. Turton K, Parks HJ, Zarodkiewicz P, Hamad MA, Dwane R, Parau G, et al. The Achromobacter
678 type 3 secretion system drives pyroptosis and immunopathology via independent activation of
679 NLRC4 and NLRP3 inflammasomes. Cell Rep. 2023;42(8):113012.
680 12. Pickrum AM, Riegert MO, Wells C, Brockman K, Frank DW. The In Vitro Replication Cycle of
681 Achromobacter xylosoxidans and Identification of Virulence Genes Associated with Cytotoxicity in
682 Macrophages. Microbiol Spectr. 2022;10(4):e0208322.
683 13. Li X, Hu Y, Gong J, Zhang L, Wang G. Comparative genome characterization of
684 Achromobacter members reveals potential genetic determinants facilitating the adaptation to a
685 pathogenic lifestyle. Appl Microbiol Biotechnol. 2013;97(14):6413-25.
686 14. Pickrum AM, DeLeon O, Dirck A, Tessmer MH, Riegert MO, Biller JA, et al. Achromobacter
687 xylosoxidans Cellular Pathology Is Correlated with Activation of a Type III Secretion System. Infect
688 Immun. 2020;88(7).
689 15. Le Goff M, Vastel M, Lebrun R, Mansuelle P, Diarra A, Grandjean T, et al. Characterization of
690 the Achromobacter xylosoxidans Type VI Secretion System and Its Implication in Cystic Fibrosis.
691 Front Cell Infect Microbiol. 2022;12:859181.
692 16. Troisfontaines P, Cornelis GR. Type III secretion: more systems than you think. Physiology
693 (Bethesda). 2005;20:326-39.
694 17. Weyrich LS, Rolin OY, Muse SJ, Park J, Spidale N, Kennett MJ, et al. A Type VI secretion
695 system encoding locus is required for Bordetella bronchiseptica immunomodulation and persistence
696 in vivo. PLoS One. 2012;7(10):e45892.
697 18. Nolan LM, Allsopp LP. Antimicrobial Weapons of Pseudomonas aeruginosa. Adv Exp Med
698 Biol. 2022;1386:223-56.

699 19. Li X, Hu Y, Gong J, Zhang L, Wang G. Comparative genome characterization of
700 Achromobacter members reveals potential genetic determinants facilitating the adaptation to a
701 pathogenic lifestyle. Applied Microbiology and Biotechnology. 2013;97(14):6413-25.
702 20. Aggarwal S, Garcia-Telles N, Aggarwal G, Lavie C, Lippi G, Henry BM. Clinical features,
703 laboratory characteristics, and outcomes of patients hospitalized with coronavirus disease 2019
704 (COVID-19): Early report from the United States. Diagnosis (Berl). 2020;7(2):91-6.
705 21. Lorenz A, Preusse M, Bruchmann S, Pawar V, Grahl N, Pils MC, et al. Importance of flagella in
706 acute and chronic Pseudomonas aeruginosa infections. Environ Microbiol. 2019;21(3):883-97.
707 22. Isler B, Kidd TJ, Stewart AG, Harris P, Paterson DL. Achromobacter Infections and Treatment
708 Options. Antimicrob Agents Chemother. 2020;64(11).
709 23. Swenson CE, Sadikot RT. Achromobacter respiratory infections. Ann Am Thorac Soc.
710 2015;12(2):252-8.
711 24. Hu Y, Zhu Y, Ma Y, Liu F, Lu N, Yang X, et al. Genomic insights into intrinsic and acquired drug
712 resistance mechanisms in Achromobacter xylosoxidans. Antimicrob Agents Chemother.
713 2015;59(2):1152-61.
714 25. Khaledi A, Weimann A, Schniederjans M, Asgari E, Kuo TH, Oliver A, et al. Predicting
715 antimicrobial resistance in Pseudomonas aeruginosa with machine learning-enabled molecular
716 diagnostics. EMBO Mol Med. 2020;12(3):e10264.
717 26. Hyun JC, Kavvas ES, Monk JM, Palsson BO. Machine learning with random subspace
718 ensembles identifies antimicrobial resistance determinants from pan-genomes of three pathogens.
719 PLoS Comput Biol. 2020;16(3):e1007608.
720 27. Kavvas ES, Catoiu E, Mih N, Yurkovich JT, Seif Y, Dillon N, et al. Machine learning and
721 structural analysis of Mycobacterium tuberculosis pan-genome identifies genetic signatures of
722 antibiotic resistance. Nat Commun. 2018;9(1):4306.
723 28. Nguyen M, Long SW, McDermott PF, Olsen RJ, Olson R, Stevens RL, et al. Using Machine
724 Learning To Predict Antimicrobial MICs and Associated Genomic Features for Nontyphoidal
725 Salmonella. J Clin Microbiol. 2019;57(2).
726 29. Ray S, Flemming LK, Scudder CJ, Ly MA, Porterfield HS, Smith RD, et al. Comparative
727 phenotypic and genotypic antimicrobial susceptibility surveillance in Achromobacter spp. through
728 whole genome sequencing. Microbiol Spectr. 2025;13(4):e0252724.
729 30. Meier-Kolthoff JP, Carbasse JS, Peinado-Olarte RL, Goker M. TYGS and LPSN: a database
730 tandem for fast and reliable genome-based classification and nomenclature of prokaryotes. Nucleic
731 Acids Res. 2022;50(D1):D801-D7.
732 31. Kalantar KL, Carvalho T, de Bourcy CFA, Dimitrov B, Dingle G, Egger R, et al. IDseq-An open
733 source cloud-based pipeline and analysis service for metagenomic pathogen detection and
734 monitoring. Gigascience. 2020;9(10).
735 32. Bador J, Neuwirth C, Grangier N, Muniz M, Germe L, Bonnet J, et al. Role of AxyZ
736 Transcriptional Regulator in Overproduction of AxyXY-OprZ Multidrug Efflux System in
737 Achromobacter Species Mutants Selected by Tobramycin. Antimicrob Agents Chemother.
738 2017;61(8).
739 33. Rees VE, Deveson Lucas DS, Lopez-Causape C, Huang Y, Kotsimbos T, Bulitta JB, et al.
740 Characterization of Hypermutator Pseudomonas aeruginosa Isolates from Patients with Cystic
741 Fibrosis in Australia. Antimicrob Agents Chemother. 2019;63(4).
742 34. Ragheb MN, Thomason MK, Hsu C, Nugent P, Gage J, Samadpour AN, et al. Inhibiting the
743 Evolution of Antibiotic Resistance. Mol Cell. 2019;73(1):157-65 e5.
744 35. Davidson AL, Chen J. ATP-binding cassette transporters in bacteria. Annu Rev Biochem.
745 2004;73:241-68.
746 36. Chen L, Zou Y, She P, Wu Y. Composition, function, and regulation of T6SS in Pseudomonas
747 aeruginosa. Microbiol Res. 2015;172:19-25.
748 37. Holban AM, Gregoire CM, Gestal MC. Conquering the host: Bordetella spp. and
749 Pseudomonas aeruginosa molecular regulators in lung infection. Front Microbiol. 2022;13:983149.

750 38. Warrier A, Satyamoorthy K, Murali TS. Quorum-sensing regulation of virulence factors in
751 bacterial biofilm. Future Microbiol. 2021;16:1003-21.
752 39. Yin R, Cheng J, Wang J, Li P, Lin J. Treatment of Pseudomonas aeruginosa infectious biofilms:
753 Challenges and strategies. Front Microbiol. 2022;13:955286.
754 40. Nielsen SM, Penstoft LN, Norskov-Lauritsen N. Motility, Biofilm Formation and Antimicrobial
755 Efflux of Sessile and Planktonic Cells of Achromobacter xylosoxidans. Pathogens. 2019;8(1).
756 41. Passos da Silva D, Matwichuk ML, Townsend DO, Reichhardt C, Lamba D, Wozniak DJ, et al.
757 The Pseudomonas aeruginosa lectin LecB binds to the exopolysaccharide Psl and stabilizes the
758 biofilm matrix. Nat Commun. 2019;10(1):2183.
759 42. Starkey M, Hickman JH, Ma L, Zhang N, De Long S, Hinz A, et al. Pseudomonas aeruginosa
760 rugose small-colony variants have adaptations that likely promote persistence in the cystic fibrosis
761 lung. J Bacteriol. 2009;191(11):3492-503.
762 43. Kazmierczak BI, Schniederberend M, Jain R. Cross-regulation of Pseudomonas motility
763 systems: the intimate relationship between flagella, pili and virulence. Curr Opin Microbiol.
764 2015;28:78-82.
765 44. Feldman M, Bryan R, Rajan S, Scheffler L, Brunnert S, Tang H, et al. Role of flagella in
766 pathogenesis of Pseudomonas aeruginosa pulmonary infection. Infect Immun. 1998;66(1):43-51.
767 45. Soscia C, Hachani A, Bernadac A, Filloux A, Bleves S. Cross talk between type III secretion and
768 flagellar assembly systems in Pseudomonas aeruginosa. J Bacteriol. 2007;189(8):3124-32.
769 46. Planet PJ. Adaptation and Evolution of Pathogens in the Cystic Fibrosis Lung. J Pediatric
770 Infect Dis Soc. 2022;11(Supplement_2):S23-S31.
771 47. Schniederberend M, Abdurachim K, Murray TS, Kazmierczak BI. The GTPase activity of FlhF is
772 dispensable for flagellar localization, but not motility, in Pseudomonas aeruginosa. J Bacteriol.
773 2013;195(5):1051-60.
774 48. Lloyd CJ, Klose KE. The Vibrio Polar Flagellum: Structure and Regulation. Adv Exp Med Biol.
775 2023;1404:77-97.
776 49. Blum M, Andreeva A, Florentino LC, Chuguransky SR, Grego T, Hobbs E, et al. InterPro: the
777 protein sequence classification resource in 2025. Nucleic Acids Res. 2025;53(D1):D444-D56.
778 50. Bange G, Petzold G, Wild K, Parlitz RO, Sinning I. The crystal structure of the third signal-
779 recognition particle GTPase FlhF reveals a homodimer with bound GTP. Proc Natl Acad Sci U S A.
780 2007;104(34):13621-5.
781 51. Zhang K, He J, Cantalano C, Guo Y, Liu J, Li C. FlhF regulates the number and configuration of
782 periplasmic flagella in Borrelia burgdorferi. Mol Microbiol. 2020;113(6):1122-39.
783 52. Balaban M, Joslin SN, Hendrixson DR. FlhF and its GTPase activity are required for distinct
784 processes in flagellar gene regulation and biosynthesis in Campylobacter jejuni. J Bacteriol.
785 2009;191(21):6602-11.
786 53. Jumper J, Evans R, Pritzel A, Green T, Figurnov M, Ronneberger O, et al. Highly accurate
787 protein structure prediction with AlphaFold. Nature. 2021;596(7873):583-9.
788 54. Papalia M, Figueroa-Espinosa R, Steffanowski C, Barberis C, Almuzara M, Barrios R, et al.
789 Expansion and improvement of MALDI-TOF MS databases for accurate identification of
790 Achromobacter species. J Microbiol Methods. 2020;172:105889.
791 55. Mosquera-Rendon J, Rada-Bravo AM, Cardenas-Brito S, Corredor M, Restrepo-Pineda E,
792 Benitez-Paez A. Pangenome-wide and molecular evolution analyses of the Pseudomonas aeruginosa
793 species. Bmc Genomics. 2016;17:45.
794 56. Abram KZ, Jun SR, Udaondo Z. Pseudomonas aeruginosa Pangenome: Core and Accessory
795 Genes of a Highly Resourceful Opportunistic Pathogen. Adv Exp Med Biol. 2022;1386:3-28.
796 57. Thorell K, Muñoz-Ramírez ZY, Wang D, Sandoval-Motta S, Boscolo Agostini R, Ghirotto S, et
797 al. The Helicobacter pylori Genome Project: insights into H. pylori population structure from analysis
798 of a worldwide collection of complete genomes. Nature Communications. 2023;14(1).
799 58. Salama NR, Shepherd B, Falkow S. Global transposon mutagenesis and essential gene
800 analysis of Helicobacter pylori. J Bacteriol. 2004;186(23):7926-35.

801 59. Bador J, Amoureux L, Duez J-M, Drabowicz A, Siebor E, Llanes C, et al. First Description of an
802 RND-Type Multidrug Efflux Pump in Achromobacter xylosoxidans, AxyABM. Antimicrobial Agents and
803 Chemotherapy. 2011;55(10):4912-4.
804 60. Bador J, Amoureux L, Blanc E, Neuwirth C. Innate Aminoglycoside Resistance of
805 Achromobacter xylosoxidans Is Due to AxyXY-OprZ, an RND-Type Multidrug Efflux Pump.
806 Antimicrobial Agents and Chemotherapy. 2013;57(1):603-5.
807 61. Magallon A, Bador J, Garrigos T, Demeule C, Chapelle A, Varin V, et al. Description of Two
808 Resistance-Nodulation-Cell Division Efflux Systems Involved in Acquired Antibiotic Resistance:
809 AxySUV in Achromobacter xylosoxidans and AinCDJ in Achromobacter insuavis. Antibiotics (Basel).
810 2025;14(6).
811 62. Ventero MP, Haro-Moreno JM, Molina-Pardines C, Sanchez-Bautista A, Garcia-Rivera C, Boix
812 V, et al. Role of Relebactam in the Antibiotic Resistance Acquisition in Pseudomonas aeruginosa: In
813 Vitro Study. Antibiotics (Basel). 2023;12(11).
814 63. Palomba E, Comelli A, Saluzzo F, Di Marco F, Matarazzo E, Re NL, et al. Activity of
815 imipenem/relebactam against KPC-producing Klebsiella pneumoniae and the possible role of
816 Ompk36 mutation in determining resistance: an Italian retrospective analysis. Ann Clin Microbiol
817 Antimicrob. 2025;24(1):23.
818 64. Holland IB, Schmitt L, Young J. Type 1 protein secretion in bacteria, the ABC-transporter
819 dependent pathway (review). Mol Membr Biol. 2005;22(1-2):29-39.
820 65. Korotkov KV, Sandkvist M. Architecture, Function, and Substrates of the Type II Secretion
821 System. EcoSal Plus. 2019;8(2):227-44.
822 66. Pohlner J, Halter R, Meyer TF. Neisseria gonorrhoeae IgA protease. Secretion and
823 implications for pathogenesis. Antonie Van Leeuwenhoek. 1987;53(6):479-84.
824 67. Brandon LD, Goehring N, Janakiraman A, Yan AW, Wu T, Beckwith J, et al. IcsA, a polarly
825 localized autotransporter with an atypical signal peptide, uses the Sec apparatus for secretion,
826 although the Sec apparatus is circumferentially distributed. Mol Microbiol. 2003;50(1):45-60.
827 68. Roggenkamp A, Ackermann N, Jacobi CA, Truelzsch K, Hoffmann H, Heesemann J. Molecular
828 analysis of transport and oligomerization of the Yersinia enterocolitica adhesin YadA. J Bacteriol.
829 2003;185(13):3735-44.
830 69. Tassinari M, Rudzite M, Filloux A, Low HH. Assembly mechanism of a Tad secretion system
831 secretin-pilotin complex. Nature Communications. 2023;14(1).
832 70. Cherrak Y, Flaugnatti N, Durand E, Journet L, Cascales E. Structure and Activity of the Type VI
833 Secretion System. Microbiology Spectrum. 2019;7(4):329-42.
834 71. Zhang X, Zeng W, Kong J, Huang Z, Shu H, Tang M, et al. The prevalence and mechanisms of
835 heteroresistance to ceftazidime/avibactam in KPC-producing Klebsiella pneumoniae. J Antimicrob
836 Chemother. 2024;79(8):1865-76.
837 72. Khademi SMH, Gabrielaite M, Paulsson M, Knulst M, Touriki E, Marvig RL, et al. Genomic and
838 Phenotypic Evolution of Achromobacter xylosoxidans during Chronic Airway Infections of Patients
839 with Cystic Fibrosis. mSystems. 2021;6(3).
840 73. Seabaugh JA, Anderson DM. Pathogenicity and virulence of Yersinia. Virulence.
841 2024;15(1):2316439.
842 74. Yuk MH, Harvill ET, Cotter PA, Miller JF. Modulation of host immune responses, induction of
843 apoptosis and inhibition of NF-kappaB activation by the Bordetella type III secretion system. Mol
844 Microbiol. 2000;35(5):991-1004.
845 75. Brugirard-Ricaud K, Duchaud E, Givaudan A, Girard PA, Kunst F, Boemare N, et al. Site-
846 specific antiphagocytic function of the Photorhabdus luminescens type III secretion system during
847 insect colonization. Cell Microbiol. 2005;7(3):363-71.
848 76. Resko ZJ, Suhi RF, Thota AV, Kroken AR. Evidence for intracellular Pseudomonas aeruginosa.
849 J Bacteriol. 2024;206(5):e0010924.
850 77. de Souza Santos M, Orth K. Intracellular Vibrio parahaemolyticus escapes the vacuole and
851 establishes a replicative niche in the cytosol of epithelial cells. mBio. 2014;5(5):e01506-14.

852 78. Guerra RM, Maleno FD, Figueras MJ, Pujol-Bajador I, Fernandez-Bravo A. Potential
853 Pathogenicity of Aeromonas spp. Recovered in River Water, Soil, and Vegetation from a Natural
854 Recreational Area. Pathogens. 2022;11(11).
855 79. Tessmer MH, Anderson DM, Pickrum AM, Riegert MO, Frank DW. Identification and
856 Verification of Ubiquitin-Activated Bacterial Phospholipases. J Bacteriol. 2019;201(4).
857 80. Dey S, Chakravarty A, Guha Biswas P, De Guzman RN. The type III secretion system needle,
858 tip, and translocon. Protein Sci. 2019;28(9):1582-93.
859 81. Vanderwoude J, Fleming D, Azimi S, Trivedi U, Rumbaugh KP, Diggle SP. The evolution of
860 virulence in Pseudomonas aeruginosa during chronic wound infection. Proc Biol Sci.
861 2020;287(1937):20202272.
862 82. Didelot X, Walker AS, Peto TE, Crook DW, Wilson DJ. Within-host evolution of bacterial
863 pathogens. Nat Rev Microbiol. 2016;14(3):150-62.
864 83. Uruen C, Chopo-Escuin G, Tommassen J, Mainar-Jaime RC, Arenas J. Biofilms as Promoters of
865 Bacterial Antibiotic Resistance and Tolerance. Antibiotics (Basel). 2020;10(1).
866 84. Yan J, Bassler BL. Surviving as a Community: Antibiotic Tolerance and Persistence in Bacterial
867 Biofilms. Cell Host Microbe. 2019;26(1):15-21.
868 85. Sandri A, Veschetti L, Saitta GM, Passarelli Mantovani R, Carelli M, Burlacchini G, et al.
869 Achromobacter spp. Adaptation in Cystic Fibrosis Infection and Candidate Biomarkers of
870 Antimicrobial Resistance. Int J Mol Sci. 2022;23(16).
871 86. Kurushima J, Kuwae A, Abe A. The type III secreted protein BspR regulates the virulence
872 genes in Bordetella bronchiseptica. PLoS One. 2012;7(6):e38925.
873 87. Singer HM, Kuhne C, Deditius JA, Hughes KT, Erhardt M. The Salmonella Spi1 virulence
874 regulatory protein HilD directly activates transcription of the flagellar master operon flhDC. J
875 Bacteriol. 2014;196(7):1448-57.
876 88. Colvin KM, Irie Y, Tart CS, Urbano R, Whitney JC, Ryder C, et al. The Pel and Psl
877 polysaccharides provide Pseudomonas aeruginosa structural redundancy within the biofilm matrix.
878 Environ Microbiol. 2012;14(8):1913-28.
879 89. Bolger AM, Lohse M, Usadel B. Trimmomatic: a flexible trimmer for Illumina sequence data.
880 Bioinformatics. 2014;30(15):2114-20.
881 90. Andrews S. FastQC: a quality control tool for high throughput sequence data. 2010.
882 91. Bankevich A, Nurk S, Antipov D, Gurevich AA, Dvorkin M, Kulikov AS, et al. SPAdes: a new
883 genome assembly algorithm and its applications to single-cell sequencing. J Comput Biol.
884 2012;19(5):455-77.
885 92. Gurevich A, Saveliev V, Vyahhi N, Tesler G. QUAST: quality assessment tool for genome
886 assemblies. Bioinformatics. 2013;29(8):1072-5.
887 93. Parks DH, Imelfort M, Skennerton CT, Hugenholtz P, Tyson GW. CheckM: assessing the
888 quality of microbial genomes recovered from isolates, single cells, and metagenomes. Genome Res.
889 2015;25(7):1043-55.
890 94. Richter M, Rossello-Mora R. Shifting the genomic gold standard for the prokaryotic species
891 definition. Proc Natl Acad Sci U S A. 2009;106(45):19126-31.
892 95. Seemann T. Prokka: rapid prokaryotic genome annotation. Bioinformatics.
893 2014;30(14):2068-9.
894 96. Tonkin-Hill G, MacAlasdair N, Ruis C, Weimann A, Horesh G, Lees JA, et al. Producing
895 polished prokaryotic pangenomes with the Panaroo pipeline. Genome Biol. 2020;21(1):180.
896 97. Hall BG, Nisbet J. Building Phylogenetic Trees From Genome Sequences With kSNP4. Mol
897 Biol Evol. 2023;40(11).
898 98. Stamatakis A. RAxML version 8: a tool for phylogenetic analysis and post-analysis of large
899 phylogenies. Bioinformatics. 2014;30(9):1312-3.
900 99. Letunic I, Bork P. Interactive Tree of Life (iTOL) v6: recent updates to the phylogenetic tree
901 display and annotation tool. Nucleic Acids Res. 2024;52(W1):W78-W82.

902 100. Page AJ, Taylor B, Delaney AJ, Soares J, Seemann T, Keane JA, et al. SNP-sites: rapid efficient
903 extraction of SNPs from multi-FASTA alignments. Microb Genom. 2016;2(4):e000056.
904 101. Minh BQ, Schmidt HA, Chernomor O, Schrempf D, Woodhams MD, von Haeseler A, et al. IQ-
905 TREE 2: New Models and Efficient Methods for Phylogenetic Inference in the Genomic Era. Mol Biol
906 Evol. 2020;37(5):1530-4.
907 102. Yahara K, Didelot X, Ansari MA, Sheppard SK, Falush D. Efficient inference of recombination
908 hot regions in bacterial genomes. Mol Biol Evol. 2014;31(6):1593-605.
909 103. Browning BL, Browning SR. A unified approach to genotype imputation and haplotype-phase
910 inference for large data sets of trios and unrelated individuals. Am J Hum Genet. 2009;84(2):210-23.
911 104. Lawson DJ, Hellenthal G, Myers S, Falush D. Inference of population structure using dense
912 haplotype data. PLoS Genet. 2012;8(1):e1002453.
913 105. Yahara K, Furuta Y, Oshima K, Yoshida M, Azuma T, Hattori M, et al. Chromosome painting in
914 silico in a bacterial species reveals fine population structure. Mol Biol Evol. 2013;30(6):1454-64.
915 106. Abby SS, Cury J, Guglielmini J, Neron B, Touchon M, Rocha EP. Identification of protein
916 secretion systems in bacterial genomes. Sci Rep. 2016;6:23080.
917 107. Katoh K, Standley DM. MAFFT multiple sequence alignment software version 7:
918 improvements in performance and usability. Mol Biol Evol. 2013;30(4):772-80.
919 108. Otsu N. A Threshold Selection Method from Gray-Level Histograms. IEEE Transactions on
920 Systems, Man, and Cybernetics. 1979;9(1):62-6.
921 109. Jones P, Binns D, Chang HY, Fraser M, Li W, McAnulla C, et al. InterProScan 5: genome-scale
922 protein function classification. Bioinformatics. 2014;30(9):1236-40.

923

924 ## 10. Figures and tables

925 **Figure 1. Geographic distribution, collection sources, and phylogenetic relationships of**
926 ***Achromobacter xylosoxidans* isolates used in this study.** (A) Number of isolates collected
927 from different countries worldwide and their respective collection sources in the NCBI
928 dataset. (B) Collection sources of *A. xylosoxidans* NIH isolates included in this study.
929 Respiratory isolates include both cystic fibrosis (CF) and non-CF patient samples. (C)
930 Phylogenetic tree of 22 curated sequences of *A. xylosoxidans* NIH isolates.

931

932 **Figure 2: Frequency of antibiotic resistance in NIH isolates.** (A) Antibiotic resistance in NIH clinical
933 isolates: CZA (Ceftazidime/Avibactam), C/T (Ceftolozane/Tazobactam), IMR (Imipenem/Relebactam),
934 MERO (Meropenem), AZT/ATM (Aztreonam), FEP (Cefepime), TAZ (Ceftazidime), CIP (Ciprofloxacin),
935 IMI (Imipenem), LEVO (Levofloxacin), PT4/TZP (Piperacillin/Tazobactam), and SXT

936 (Trimethoprim/Sulfamethoxazole). Black: resistance, gray: intermediate, white: susceptible. (B)
937 Percentage of isolates resistance to each antibiotic was shown.
938
939 **Figure 3: Type III secretion system (T3SS) phylogeny and structure**. (A) Phylogenetic tree of T3SS
940 families constructed from aligned amino acid sequences of SctN and its homologs. (B) Predicted
941 structure of YscN from *Achromobacter xylosoxidans*. (C) Superimposed predicted structures of *A.*
942 *xylosoxidans* YscN (orange) and *Pseudomonas aeruginosa* PA14 PscN (blue).
943
944 **Figure 4: Cytotoxicity, adherence and uptake of *A. xylosoxidans* clinical isolates in macrophage.**
945 (A) Cell death of J774A.1 macrophages infected with selected *A. xylosoxidans* clinical isolates over
946 time. (B) Cell death of J774A.1 macrophages infected with different *A. xylosoxidans* clinical isolates
947 at 5 hours after infection (hpi). (C) Adherence and (D) internalization of selected *A.*
948 *xylosoxidans* isolates. Percent of inoculum is shown. (E) Cell death of J774A.1 macrophages infected
949 with cytotoxic isolates in the presence or absence of cytochalasin D. Percent cell death, calculated as
950 the ratio of dead to total cells, is shown. Different symbol shapes represent independent biological
951 replicates. One-way ANOVA with multiple comparison test was used. **** P-val <0.0001, *** P-val
952 <0.0002, ** P-val <0.002, *P-val <0.05.
953
954 **Figure 5: Biofilm formation by *A. xylosoxidans* clinical isolates.** PA01 Δ*wspF*Δ*pelA*Δ*pslBCD* was used
955 as a negative control and PA01 Δ*wspF* was used as a positive control. Different symbol shapes
956 represent independent biological replicates. The experiment was done in at least three technical
957 replicates. Kruskal-Wallis test was done followed by Dunn's multiple comparisons to correct for
958 multiple comparison. **** P-val <0.0001, *** P-val <0.0002, ** P-val <0.002, *P-val <0.05.
959
960 **Figure 6: *A. xylosoxidans* motility.** (A) *A. xylosoxidans* demonstrates substantial differences in
961 flagellar motility among clinical isolates. (B) FlhF is a 937 amino acid (aa) protein that contains a FlhF

962 family domain (aa 190-415) and an SRP54 domain (aa 327-522), based on InterProscan (109). In
963 isolate NIH-016-3, FlhF carries a point mutation at position 330, resulting in a Y330H substitution
964 within the SRP54 domain. (C) Mutation Y330H results in a predicted displacement of V229 (Green) as
965 determined by modeling in Alphafold (Blue: NIH-016-2 FlhF, Red: NIH-016-3 FlhF). (D) Alignment of
966 monomeric NIH-016-2 FlhF (Blue) to homodimerized NIH-016-2 FlhF (Yellow). (E) Alignment of NIH-
967 016-2 (Blue) to *B. subtilis* FlhF (Pink) with bound GTP (Red).
968
969
970
971

972

Table 1: Core genes in *Achromobacter xylosoxidans*

* Rare genes that occurs in less than 15% of isolates are not counted in the total genes to avoid underestimate the core gene for each genome.

Description	counts
Core genes (99% <= strains <= 100%)	2216
Soft core genes (95% <= strains < 99%)	1274
Shell genes (15% <= strains < 95%)	2943
Cloud genes (0% <= strains < 15%)	22279
Total genes *(15% <= strains <= 100%)	6433

973

974

975 **Table 2: Summary of secretion system, motility, cytotoxicity, and biofilm of *A. xylosoxidans***

976 **isolates.** Three intra-host isolate series were highlighted in different colors. NIH-016-1 and NIH-018-

977 3 were included in the table for the analysis of intra-host samples, while the genome sequences

978 were omitted in the phylogenetic analysis due to contamination issue.

979 [*]motility in mm^2

980 [#]cytotoxicity: percent cell death at 5 hours after infection

981 [$] biofilm: Absorbance 595nm of crystal violet stained biofilm

982 [**]AR: Total number of antibiotics that each isolate is resistant to out of 12 tested

983 [##] BAL: Bronchoalveolar lavage, AXL: Autopsy of the lung

Isolate	T1SS	T2SS	T3SS	T4SS	T5SS	T6SS	Tad	flagella	motility[*]	cytotoxicity[#]	presence of AxoU	Biofilm[$]	AR[**]	collection date	Source[##]
NIH-003-1	Y	Y	Y	Y	Y	Y	Y	Y	16.9	5.9	yes	0.39	2	12/17/17	Wound
NIH-005-4	Y	Y	Y	Y	Y	Y	Y	Y	17.2	9.7	yes	0.34	2	10/10/14	Sputum
NIH-005-3	Y	Y	Y	Y	Y	Y	Y	Y	1.9	5.6	yes	0.11	9	10/30/16	BAL
NIH-005-2	Y	Y	Y	Y	Y	Y	Y	Y	2.1	3.9	yes	0.12	10	11/10/16	Perirectal
NIH-009-1	Y	Y	Y	N	Y	Y	Y	Y	9.5	2.8	yes	0.29	2	8/29/16	BAL
NIH-010-6	Y	Y	Y	Y	Y	Y	Y	Y	6.7	3.5	yes	0.20	5	9/4/12	Skin lesion
NIH-010-4	Y	Y	Y	Y	Y	Y	Y	Y	0.6	9.8	yes	0.19	5	7/26/13	BAL
NIH-010-3	Y	Y	Y	Y	Y	Y	Y	Y	0.7	1.8	yes	0.31	7	7/5/14	Sputum
NIH-014-1	Y	Y	Y	Y	Y	Y	Y	Y	15.1	3.1	yes	0.31	3	11/16/15	Autopsy lung

NIH-016-2	Y	Y	Y	Y	Y	Y	Y	Y	13.5	7.5	yes	0.31	3	7/15/14	Sputum
NIH-016-3	Y	Y	Y	Y	Y	Y	Y	Y	0.7	2.5	yes	0.34	11	2/11/15	Sputum
NIH-016-1	Y	Y	Y	Y	Y	Y	Y	Y	0.6805	5.4	yes	0.52	11	2/24/16	Sputum
NIH-017-1	Y	Y	Y	Y	Y	Y	Y	Y	0.6	5.7	yes	0.30	2	1/8/15	Nephrostomy urine
NIH-018-3	Y	Y	Y	Y	Y	Y	Y	Y	17.4	15.5	Yes	0.26	6	12/13/12	BAL
NIH-018-2	Y	Y	Y	Y	Y	Y	Y	Y	8.4	26.8	yes	0.21	6	11/8/13	Sputum
NIH-018-1	Y	Y	Y	Y	Y	Y	Y	Y	9.3	45.3	yes	0.47	6	1/22/14	Sputum
NIH-022-1	Y	Y	Y	Y	Y	Y	Y	Y	2.7	11.7	yes	0.25	2	12/7/12	Sputum
NIH-023-1	Y	Y	N	Y	Y	Y	Y	N	0.5	4.9	no	0.31	3	3/22/13	BAL
NIH-025-1	Y	Y	Y	Y	Y	Y	Y	Y	8.9	29.9	yes	0.38	8	11/12/13	Blood
NIH-025-3	Y	Y	Y	Y	Y	Y	Y	Y	7.1	20.1	yes	0.32	9	11/20/13	Blood
NIH-025-4	Y	Y	Y	Y	Y	Y	Y	Y	5.1	28.8	yes	0.35	9	11/22/13	axl
NIH-025-5	Y	Y	Y	Y	Y	Y	Y	Y	5.5	11.8	yes	0.38	8	11/10/13	Blood
NIH-025-6	Y	Y	Y	Y	Y	Y	Y	Y	7.1	29.6	yes	0.51	9	11/9/13	BAL
NIH-026-1	Y	Y	Y	Y	Y	Y	Y	Y	20.6	4.7	yes	0.32	2	5/1/16	Wound (l heel)
GCA_016728825.1 (reference)	Y	Y	Y	Y	Y	Y	Y	Y	ND	ND	yes	ND	ND	4/30/18	Soil

GCA_013282235.1 (GN050)	Y	Y	Y	Y	Y	Y	Y	Y	8.0	36.7	yes	0.74	ND	7/12/10	Ear effusion
GCA_013282255.1 (GN008)	Y	Y	Y	Y	Y	Y	Y	Y	0.4	3.6	yes	0.35	ND	6/29/10	Cystic fibrosis sputum

984

Table 3: Changes of the genome between NIH-016-2 and NIH-016-1, NIH-016-3. NIH-016-2 was used as a reference. The mutations listed are the common mutations between NIH-016-3 and NIH-016-1, compared to NIH-016-2.

CHROM	POS	REF	ALT	EFFECT	LOCUS_TAG	PRODUCT
CP188777	36790	A	G	missense_variant c.41A>G p.Asp14Gly	ACP6EQ_00165	AraC family transcriptional regulator
CP188777	306544	C	T	missense_variant c.106C>T p.Arg36Cys	ACP6EQ_01455	ornithine cyclodeaminase
CP188777	444497	A	G	missense_variant c.472A>G p.Ser158Gly	ACP6EQ_02080	Bug family tripartite tricarboxylate transporter substrate binding protein
CP188777	497968	A	G	missense_variant c.74T>C p.Val25Ala	ACP6EQ_02315	c-type cytochrome
CP188777	642598	C	T	missense_variant c.733G>A p.Glu245Lys	ACP6EQ_03095	bifunctional hydroxymethylpyrimidine kinase/phosphomethylpyrimidine kinase
CP188777	755449	C	G	missense_variant c.700G>C p.Gly234Arg	ACP6EQ_03575	DUF342 domain-containing protein
CP188777	785311	A	G	missense_variant c.1313T>C p.Leu438Pro	ACP6EQ_03715	ribonuclease catalytic domain-containing protein
CP188777	896554	T	C	missense_variant c.443T>C p.Val148Ala	ACP6EQ_04250	MFS transporter
CP188777	1117935	C	T	missense_variant c.32G>A p.Gly11Asp	ACP6EQ_05315	polynucleotide adenylyltransferase PcnB
CP188777	1123581	A	T	missense_variant c.695T>A p.Leu232Gln	ACP6EQ_05345	DNA mismatch repair endonuclease MutL
CP188777	1351955	T	G	missense_variant c.700A>C p.Thr234Pro	ACP6EQ_06450	tyrosine-type recombinase/integrase

CP188777	1381223	A	G	missense_variant c.511A>G p.Thr171Ala	ACP6EQ_06610	glycosyltransferase family 9 protein
CP188777	1587091	T	G	missense_variant c.86T>G p.Val29Gly	ACP6EQ_07535	multidrug efflux transcriptional repressor AxyZ
CP188777	1620551	A	G	missense_variant c.2228T>C p.Leu743Pro	ACP6EQ_07680	transcription-repair coupling factor
CP188777	1704773	C	T	missense_variant c.848G>A p.Arg283His	ACP6EQ_08075	Bug family tripartite tricarboxylate transporter substrate binding protein
CP188777	1828128	A	G	missense_variant c.4874A>G p.Tyr1625Cys	ACP6EQ_08585	hemagglutinin repeat-containing protein
CP188777	1924181	G	A	missense_variant c.98G>A p.Gly33Asp	ACP6EQ_09000	1,2-phenylacetyl-CoA epoxidase subunit PaaA
CP188777	2069911	A	AC	frameshift_variant c.278dupC p.His94fs	ACP6EQ_09695	glycolate oxidase subunit GlcE
CP188777	2107651	C	T	missense_variant c.146C>T p.Ser49Leu	ACP6EQ_09910	aromatic amino acid DMT transporter YddG
CP188777	2194430	A	G	missense_variant c.299T>C p.Val100Ala	ACP6EQ_10305	DUF3053 domain-containing protein
CP188777	2395874	A	G	missense_variant c.133A>G p.Thr45Ala	ACP6EQ_11165	DUF5339 family protein
CP188777	2494682	G	A	missense_variant c.553G>A p.Gly185Ser	ACP6EQ_11675	copper-containing nitrite reductase
CP188777	2510615	G	C	missense_variant c.88G>C p.Val30Leu	ACP6EQ_11745	SDR family oxidoreductase
CP188777	2516449	C	T	missense_variant c.451C>T p.Arg151Cys	ACP6EQ_11765	class I SAM-dependent DNA methyltransferase
CP188777	2676682	C	T	missense_variant c.1264G>A p.Val422Met	ACP6EQ_12500	heavy metal translocating P-type ATPase

CP188777	3110891	T	C	missense_variant c.278A>G p.Tyr93Cys	ACP6EQ_14500	Bug family tripartite tricarboxylate transporter substrate binding protein
CP188777	3111709	A	G	missense_variant c.422A>G p.Tyr141Cys	ACP6EQ_14505	LysR family transcriptional regulator
CP188777	3172298	A	G	missense_variant c.415T>C p.Cys139Arg	ACP6EQ_14805	GMC family oxidoreductase
CP188777	3444638	G	A	missense_variant c.592C>T p.Arg198Cys	ACP6EQ_16040	ABC transporter substrate-binding protein
CP188777	3770678	A	G	missense_variant c.1001T>C p.Val334Ala	ACP6EQ_17480	D-cysteine desulfhydrase family protein
CP188777	3793425	AG	GC	missense_variant c.46_47delCTinsGC p.Leu16Ala	ACP6EQ_17565	cystathionine gamma-synthase family protein
CP188777	4560728	G	GC	frameshift_variant c.839dupG p.Val281fs	ACP6EQ_20870	molybdopterin cofactor-binding domain-containing protein
CP188777	4914304	T	C	missense_variant c.1876A>G p.Thr626Ala	ACP6EQ_22475	TonB-dependent receptor
CP188777	4918789	T	C	missense_variant c.230T>C p.Val77Ala	ACP6EQ_22490	response regulator transcription factor
CP188777	4951892	G	GC	frameshift_variant c.73dupG p.Ala25fs	ACP6EQ_22700	PBSX family phage terminase large subunit
CP188777	5023271	T	C	missense_variant c.464A>G p.Tyr155Cys	ACP6EQ_23155	4-hydroxythreonine-4-phosphate dehydrogenase PdxA
CP188777	5074135	A	G	missense_variant c.818T>C p.Val273Ala	ACP6EQ_23405	ABC transporter substrate-binding protein
CP188777	5144580	A	G	missense_variant c.74T>C p.Val25Ala	ACP6EQ_23735	acetyl-CoA hydrolase/transferase family protein

CP188777	5147082	G	GC	frameshift_variant c.1181dupC p.Pro395fs	ACP6EQ_23745	DUF3772 domain-containing protein
CP188777	5368021	A	G	missense_variant c.358A>G p.Thr120Ala	ACP6EQ_24820	protein translocase subunit SecD
CP188777	5525409	T	C	missense_variant c.1396A>G p.Thr466Ala	ACP6EQ_25620	TonB-dependent siderophore receptor
CP188777	5614531	A	G	missense_variant c.10T>C p.Cys4Arg	ACP6EQ_26035	Bug family tripartite tricarboxylate transporter substrate binding protein
CP188777	5749106	G	GC	frameshift_variant c.1721dupG p.Ala575fs	ACP6EQ_26625	autotransporter domain-containing protein
CP188777	5968107	A	G	missense_variant c.179A>G p.Asn60Ser	ACP6EQ_27535	prolyl aminopeptidase
CP188777	5994882	T	C	missense_variant c.439A>G p.Ser147Gly	ACP6EQ_27665	RNA polymerase sigma factor
CP188777	6041085	G	GC	frameshift_variant c.25dupC p.Leu9fs	ACP6EQ_27890	response regulator
CP188777	6213780	T	C	missense_variant c.1043T>C p.Val348Ala	ACP6EQ_28685	30S ribosomal protein S12 methylthiotransferase RimO
CP188777	6348240	C	T	missense_variant c.104G>A p.Gly35Asp	ACP6EQ_29305	alpha/beta fold hydrolase
CP188777	6398223	T	C	missense_variant c.688T>C p.Tyr230His	ACP6EQ_29565	N-acetyl sugar amidotransferase
CP188777	6419572	A	ACG	frameshift_variant c.481_482dupGC p.Tyr162fs	ACP6EQ_29660	dTDP-4-amino-4,6-dideoxygalactose transaminase
CP188777	6486625	CG	C	frameshift_variant c.421delG p.Glu141fs	ACP6EQ_29965	HIT family protein
CP188777	6585839	C	T	missense_variant c.1195G>A p.Glu399Lys	ACP6EQ_30490	catalase

985

986

987

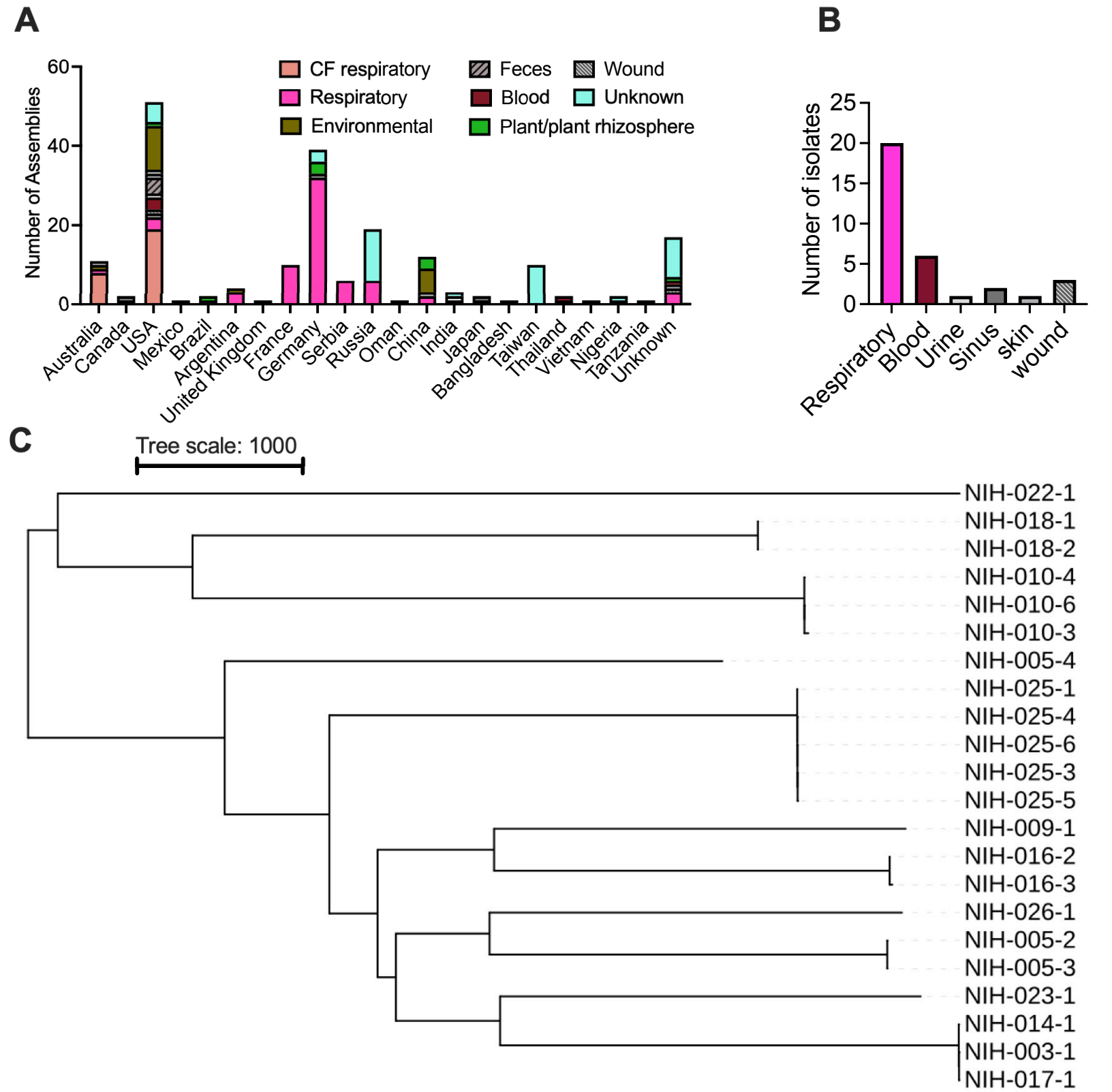
A
Number of Assemblies
60
40
20
0
CF respiratory
Respiratory
Environmental
Feces
Blood
Plant/plant rhizosphere
Wound
Unknown
Australia
Canada
USA
Mexico
Brazil
Argentina
United Kingdom
France
Germany
Serbia
Russia
Oman
China
India
Japan
Bangladesh
Taiwan
Thailand
Vietnam
Nigeria
Tanzania
Unknown
B
Number of isolates
25
20
15
10
5
0
Respiratory
Blood
Urine
Sinus
skin
wound
C
Tree scale: 1000
NIH-022-1
NIH-018-1
NIH-018-2
NIH-010-4
NIH-010-6
NIH-010-3
NIH-005-4
NIH-025-1
NIH-025-4
NIH-025-6
NIH-025-3
NIH-025-5
NIH-009-1
NIH-016-2
NIH-016-3
NIH-026-1
NIH-005-2
NIH-005-3
NIH-023-1
NIH-014-1
NIH-003-1
NIH-017-1

A

Isolate/ antibiotic	CZA	C/T	IMR	MERO	AZT/ ATM	FEP	TAZ	CIP	IMI	LEVO	PT4/ TZP	SXT
NIH-003-1												
NIH-005-4												
NIH-005-3												
NIH-005-2												
NIH-009-1												
NIH-010-6												
NIH-010-4												
NIH-010-3												
NIH-014-1												
NIH-016-2												
NIH-016-3												
NIH-017-1												
NIH-018-2												
NIH-018-1												
NIH-022-1												
NIH-023-1												
NIH-025-6												
NIH-025-5												
NIH-025-1												
NIH-025-3												
NIH-025-4												
NIH-026-1												

B

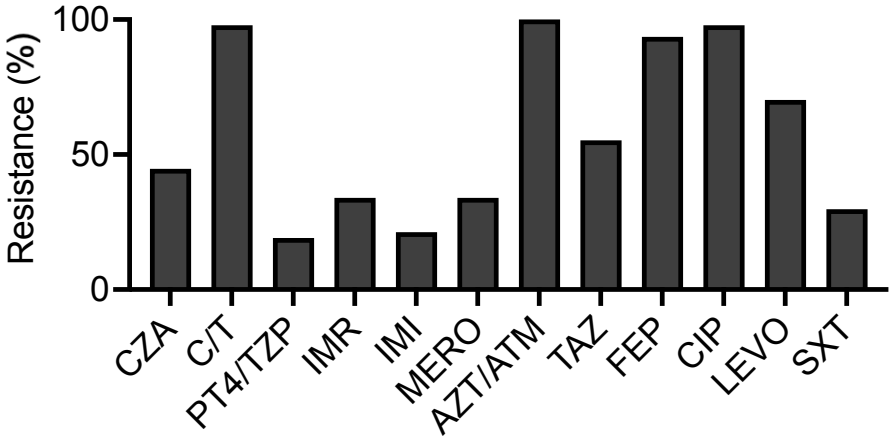

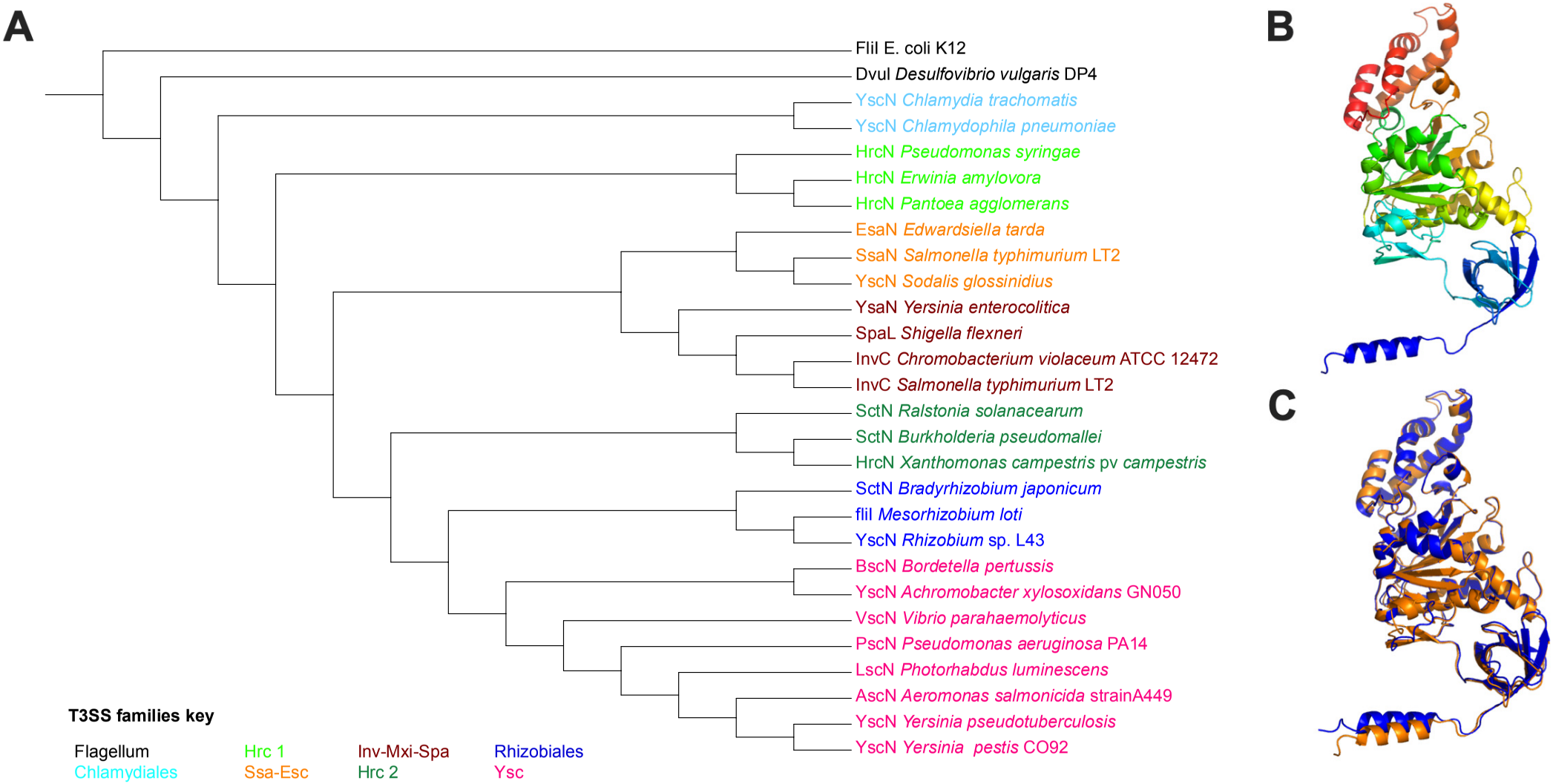
A
FliI E. coli K12
DvuI Desulfovibrio vulgaris DP4
YscN Chlamydia trachomatis
YscN Chlamydophila pneumoniae
HrcN Pseudomonas syringae
HrcN Erwinia amylovora
HrcN Pantoea agglomerans
EsaN Edwardsiella tarda
SsaN Salmonella typhimurium LT2
YscN Sodalis glossinidius
YsaN Yersinia enterocolitica
SpaL Shigella flexneri
InvC Chromobacterium violaceum ATCC 12472
InvC Salmonella typhimurium LT2
SctN Ralstonia solanacearum
SctN Burkholderia pseudomallei
HrcN Xanthomonas campestris pv campestris
SctN Bradyrhizobium japonicum
fliI Mesorhizobium loti
YscN Rhizobium sp. L43
BscN Bordetella pertussis
YscN Achromobacter xylosoxidans GN050
VscN Vibrio parahaemolyticus
PscN Pseudomonas aeruginosa PA14
LscN Photorhabdus luminescens
AscN Aeromonas salmonicida strainA449
YscN Yersinia pseudotuberculosis
YscN Yersinia pestis CO92
T3SS families key
Flagellum
Chlamydiales
Hrc 1
Ssa-Esc
Inv-Mxi-Spa
Hrc 2
Rhizobiales
Ysc
B
C

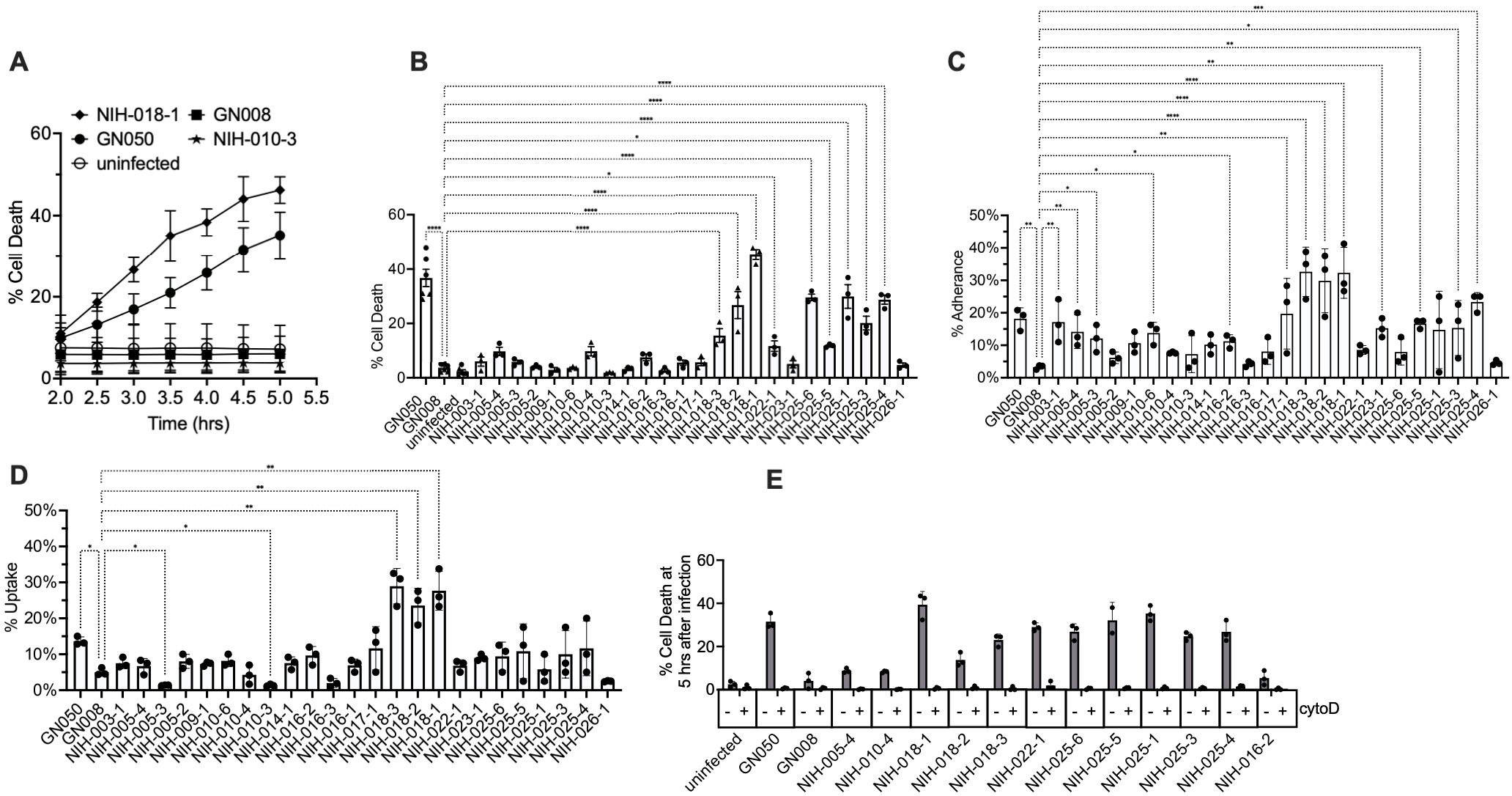
A
NIH-018-1
GN008
GN050
NIH-010-3
uninfected
% Cell Death
Time (hrs)
B
% Cell Death
C
% Adherance
D
% Uptake
E
% Cell Death at 5 hrs after infection
cytoD
GN050
GN008
uninfected
NIH-003-1
NIH-005-4
NIH-005-3
NIH-005-2
NIH-009-1
NIH-010-6
NIH-010-4
NIH-010-3
NIH-014-1
NIH-016-2
NIH-016-3
NIH-016-1
NIH-017-1
NIH-018-3
NIH-018-2
NIH-018-1
NIH-022-1
NIH-023-1
NIH-025-6
NIH-025-5
NIH-025-1
NIH-025-3
NIH-025-4
NIH-026-1
NIH-016-2

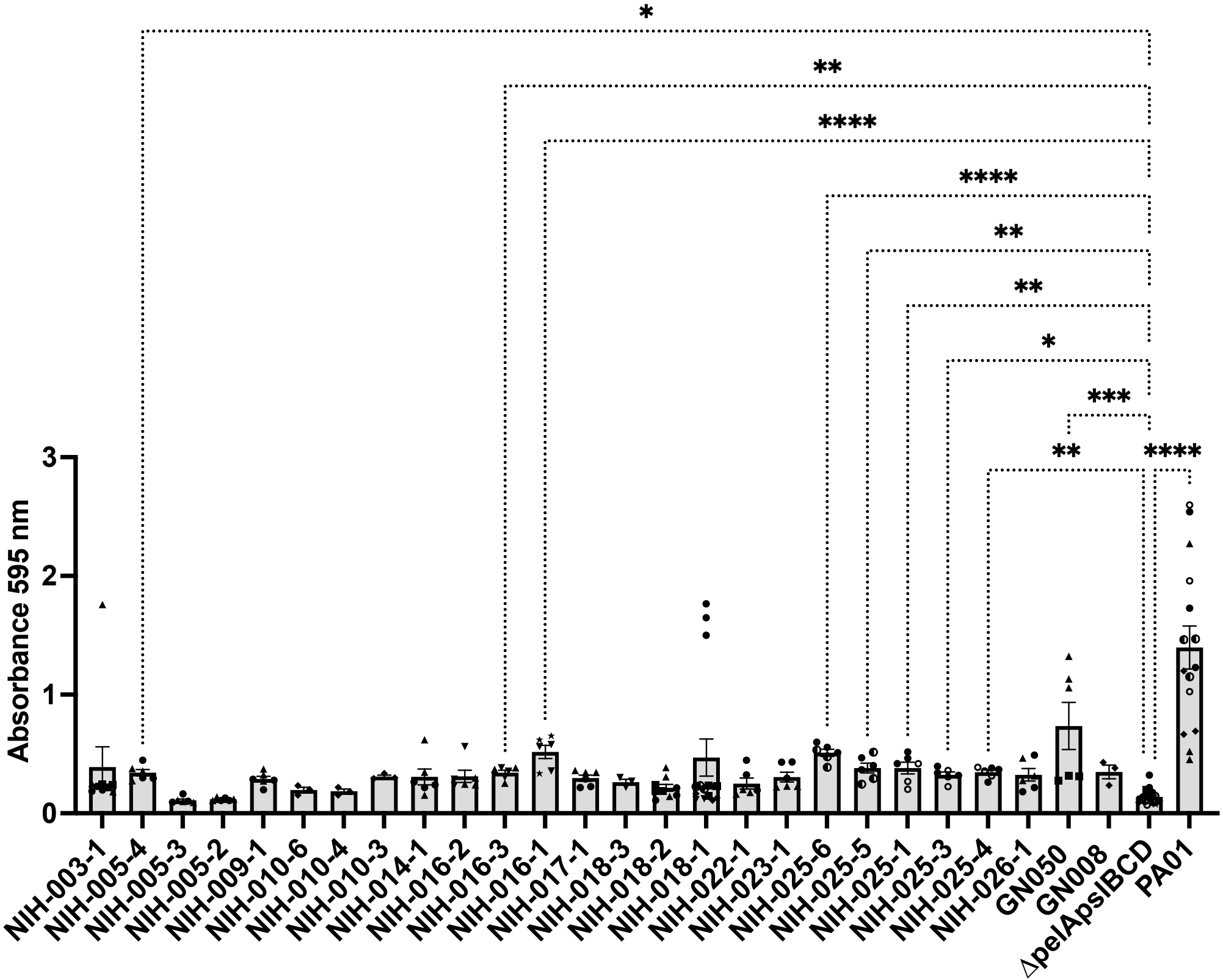
Absorbance 595 nm
0
1
2
3
*
**
****
****
**
**
*
***
**
****
NIH-003-1
NIH-005-4
NIH-005-3
NIH-005-2
NIH-009-1
NIH-010-6
NIH-010-4
NIH-010-3
NIH-014-1
NIH-016-2
NIH-016-3
NIH-016-1
NIH-017-1
NIH-018-3
NIH-018-2
NIH-018-1
NIH-022-1
NIH-023-1
NIH-025-6
NIH-025-5
NIH-025-1
NIH-025-3
NIH-025-4
NIH-026-1
GN050
GN008
ΔpelApslBCD
PA01

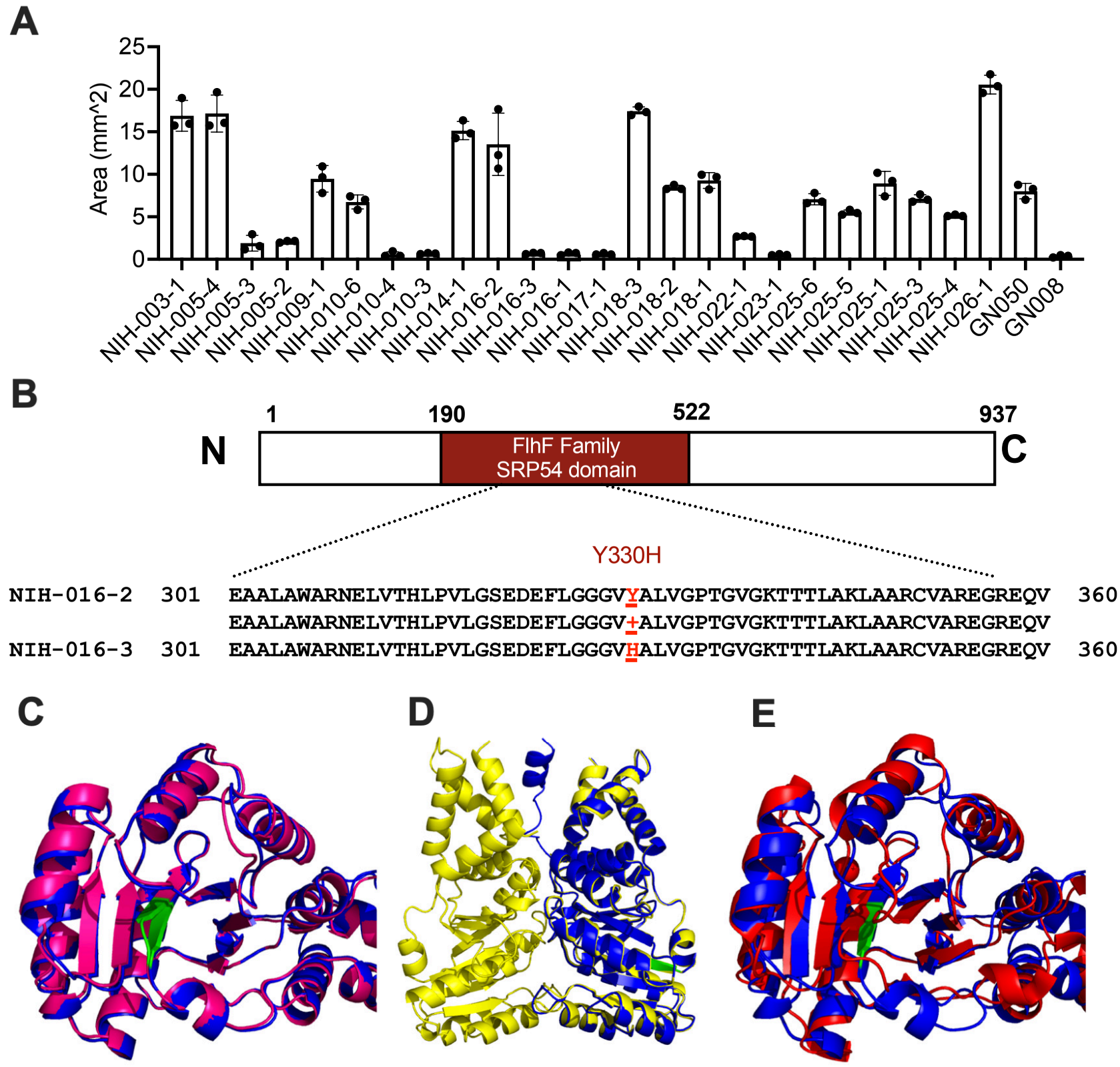
A
Area (mm^2)
25
20
15
10
5
0
NIH-003-1
NIH-005-4
NIH-005-3
NIH-005-2
NIH-009-1
NIH-010-6
NIH-010-4
NIH-010-3
NIH-014-1
NIH-016-2
NIH-016-3
NIH-016-1
NIH-017-1
NIH-018-3
NIH-018-2
NIH-018-1
NIH-022-1
NIH-023-1
NIH-025-6
NIH-025-5
NIH-025-1
NIH-025-3
NIH-025-4
NIH-026-1
GN050
GN008
B
1
190
522
937
N
FlhF Family
SRP54 domain
C
Y330H
NIH-016-2 301 EAALAWARNELVTHLPVLGSEDEFLGGGVYALVGPTGVGKTTTLAKLAARCVAREGREQV 360
EAALAWARNELVTHLPVLGSEDEFLGGGV+ALVGPTGVGKTTTLAKLAARCVAREGREQV
NIH-016-3 301 EAALAWARNELVTHLPVLGSEDEFLGGGVHALVGPTGVGKTTTLAKLAARCVAREGREQV 360
C
D
E